Available online at www.sciencedirect.com
SCIENCE DIRECT®
ELSEVIER
International Journal of Plasticity 22 (2006) 497–535
INTERNATIONAL JOURNAL OF Plasticity
www.elsevier.com/locate/ijplas

A plane stress anisotropic plastic flow theory for orthotropic sheet metals

Wei Tong *

Department of Mechanical Engineering, 219 Becton Center, Yale University, New Haven, CT 06520-8284, United States

Received 13 December 2003
Available online 8 August 2005

Abstract

A phenomenological theory is presented for describing the anisotropic plastic flow of orthotropic polycrystalline aluminum sheet metals under plane stress. The theory uses a stress exponent, a rate-dependent effective flow strength function, and five anisotropic material functions to specify a flow potential, an associated flow rule of plastic strain rates, a flow rule of plastic spin, and an evolution law of isotropic hardening of a sheet metal. Each of the five anisotropic material functions may be represented by a truncated Fourier series based on the orthotropic symmetry of the sheet metal and their Fourier coefficients can be determined using experimental data obtained from uniaxial tension and equal biaxial tension tests. Depending on the number of uniaxial tension tests conducted, three models with various degrees of planar anisotropy are constructed based on the proposed plasticity theory for power-law strain hardening sheet metals. These models are applied successfully to describe the anisotropic plastic flow behavior of 10 commercial aluminum alloy sheet metals reported in the literature.

Keywords: Plastic flow potential; Isotropic hardening; Uniaxial tension; Equal biaxial tension

* Tel.: +1 203 432 4260; fax: +1 203 432 6775.
E-mail address: wei.tong@yale.edu.

0749-6419/$ - see front matter © 2005 Elsevier Ltd. All rights reserved.
doi:10.1016/j.ijplas.2005.04.005

1. Introduction

Many secondary forming operations of rolled sheet metal have nowadays been numerically simulated for both improving existing and developing new manufacturing technologies and for applications of these manufacturing technologies using new metal alloys such as automotive aluminum sheets. As textured sheet metals produced by hot and cold rolling exhibit significant anisotropic plastic flow characteristics, effective and accurate modeling of yielding and plastic flow behaviors of sheet metals under a general stress state or strain path has long been an important research topic in plasticity (Hill, 1948, 1950; Hosford, 1993; Hosford and Caddell, 1993). Nevertheless, existing anisotropic plasticity models such as Hill's classical quadratic theory are found to be inadequate in describing the plastic flow behavior in most of commercial aluminum sheet metals (Lademo et al., 1999; Wu et al., 2003). Research efforts have continued towards further improving the accuracy and robustness of anisotropic plasticity models of sheet metals (Hill, 1979, 1990, 1993; Graf and Hosford, 1993, 1994; Karafillis and Boyce, 1993; Barlat et al., 1997a,b, 2004, 2005; Wu et al., 1999; Wu, 2002; Van Houtte and Van Bael, 2004; Banabic et al., 2005; Chung et al., 2005; Hu, 2005).

Hill (1948, 1950) proposed an elegant anisotropic plasticity theory for orthotropic sheet metals by generalizing the classical von Mises isotropic flow potential. Hill's quadratic anisotropic flow potential is analytically very simple and captures the essence of the anisotropic plastic flow behavior by differentiating the in-plane and out-of-plane plastic deformation modes in a sheet metal. Parameters in Hill's (1948) model can also be easily determined from simple tests as they are explicitly related to material properties such as uniaxial tensile flow stress and uniaxial plastic stain ratio in a simple manner. Various new phenomenological flow potentials have since been proposed to improve Hill's (1948) anisotropic plastic flow theory (Bassani, 1977; Gotoh, 1977; Hill, 1979, 1990, 1991, 1993; Logan and Hosford, 1980; Budiansky, 1984; Jones and Gillis, 1984; Hosford, 1985; Barlat and Richmond, 1987; Barlat, 1987; Barlat and Lian, 1989; Barlat et al., 1991; Montheillet et al., 1991; Karafillis and Boyce, 1993; Lin and Ding, 1996; Barlat et al., 1997a,b, 2004, 2005; Wu et al., 1999; Wu, 2002). In general, most of these stress-based flow potentials are non-quadratic and some use rather complicated functional forms to model more effectively planar anisotropy and the "anomalous" flow behavior as exhibited in some aluminum alloys (Pearce, 1968; Woodthorpe and Pearce, 1970; Dodd and Caddell, 1984). The number of material parameters in those flow potentials in plane stress condition is usually five or more and these material parameters are often estimated using uniaxial and biaxial tensile stress–strain curves as well as uniaxial plastic strain ratios (Hill, 1993; Lin and Ding, 1996). More recently, even more generalized anisotropic flow potentials (Barlat and Richmond, 1987; Barlat, 1987; Barlat and Lian, 1989; Barlat et al., 1991; Montheillet et al., 1991; Karafillis and Boyce, 1993; Barlat et al., 1997a,b, 2004; Cao et al., 2000; Yao and Cao, 2002) have been developed using the so-called isotropic plasticity equivalent (IPE) stress tensor (Karafillis and Boyce, 1993), which is often defined as a *linearly transformed* stress tensor $\mathbf{S} = \mathbf{L}\boldsymbol{\sigma}$ (where $\boldsymbol{\sigma}$ is the Cauchy stress tensor and $\mathbf{L}$ is a four-order tensorial operator accounting for the material symmetry such as orthotropic, triclinic, monoclinic, and so on).

While the introduction of an isotropic plasticity equivalent stress tensor seems to provide a very good basis for developing general anisotropic plasticity theories, the formulation of a particular model for a given class of sheet metals such as aluminum alloys still requires additional orientation-dependent weighting functions (Barlat et al., 1997a,b) and may need either a nonlinear stress transformation or at least two isotropic plasticity equivalent stress tensors defined by two different four-order linear tensorial operators (Barlat et al., 1997b, 2004). The generalized anisotropic plasticity models using the isotropic plasticity equivalent stress tensors are analytically complicated and thus not user-friendly. The linear transformation coefficients and weighting coefficients in these generalized models are not explicitly related to easily measurable material properties as they are coupled in a highly nonlinear manner. Nonlinear equations involving these material parameters are often solved by an iterative numerical technique. The solution is found to be rather sensitive to the types of experimental data selected (Barlat et al., 2004) and is often non-unique (Cao et al., 2000) as most models admits no more than seven independent material parameters if not considering the kinematic hardening via a back stress tensor (Karafillis and Boyce, 1993; Barlat et al., 1997a,b, 2004; Cao et al., 2000). For orthotropic sheet metals that may need more than seven material parameters to accurately characterize its planar anisotropy, there have been some efforts to further extend these models (Bron and Besson, 2004; Barlat et al., 2005).

In this investigation, an anisotropic plastic theory of orthotropic sheet metals formulated in terms of the intrinsic variables of principal stresses and a loading orientation angle is presented. The constitutive equations in the theory are first summarized in Section 2 (a detailed derivation of these constitutive equations based on effective macroscopic slips is given in Appendix A of this paper for the completeness of the presentation). The procedure for determining the anisotropic material functions in the theory is detailed in Section 3 using a single equal-biaxial tension test and multiple uniaxial tension tests of a sheet metal. Three models with various degrees of planar anisotropy constructed from the theory are then used to describe the anisotropic plastic flow behavior of 10 commercial aluminum sheet metals in Section 4. A discussion about the proposed anisotropic plasticity theory and its further experimental evaluations are presented in Section 5. Conclusions are summarized in Section 6 on the current investigation of anisotropic flow modeling of aluminum sheet metals.

2. A plane-stress anisotropic plasticity theory based on macroscopic slips

As the anisotropic plasticity model is intended for sheet metal forming applications, we seek to describe the plastic *flow* behavior of sheet metals beyond the initial yielding and up to a strain level before localized necking. Similar to the reasoning given by Barlat et al. (1997a,b, 2004), Bauschinger effects and non-isotropic hardening associated with the initial yielding and small-strain anisotropy and the deformation induced significant texture changes and back-stresses associated with very large strains are not considered here (Phillips et al., 1972; Eisenberg and Yen,

1981; Karafillis and Boyce, 1993; Wu et al., 1999). Strain hardening of sheet metals will thus be considered to be proportional or isotropic but its evolution may be dependent of both the loading orientation and the stress state. Throughout this investigation, flow potentials (surfaces) instead of yield functions (surfaces) will be used to emphasize modeling of plastic flow behavior of sheet metals well beyond the initial yielding and the flow surface should be experimentally defined by the back-extrapolation method or a big offset strain (Hill, 1979; Wu, 2002).

2.1. Summary of the constitutive equations

The sheet metal material element is defined by a Cartesian material texture coordinate system in terms of the rolling direction (x), the transverse direction (y) and the normal direction (z) of an orthotropic sheet metal. A plane stress state can be described by the two principal stress components σ_1 and σ_2 in the x–y plane with $|\sigma_1| \geqslant |\sigma_2|$ and a *loading orientation angle* θ. The loading orientation angle is defined as the angle between the direction of the major principal stress component σ_1 and the rolling direction of the sheet metal. When $\sigma_1 = \sigma_2$, the principal axes of stress are set to coincide with the principal axes of strain rates, which correspond naturally to the orthotropic axes of the sheet metal. Such a selection of the principal axes of stress avoids the ambiguity of defining the loading orientation angle θ under equal biaxial loading (it is zero when $\sigma_1 = \sigma_2$). The definition of the major principal stress $|\sigma_1| \geqslant |\sigma_2|$ also excludes the consideration of the Bauschinger effect. Based on the recent developments of an anisotropic plasticity theory of sheet metals derived from the concept of effective macroscopic slips (Tong, 2005), a simplified version of that theory is proposed in the following (a detailed derivation of the constitutive equations in the original theory is given in Appendix A.)

$$\begin{aligned}\tau &= \{F(\theta)|\sigma_1|^a + G(\theta)|\sigma_2|^a + H(\theta)|\sigma_1 - \sigma_2|^a\}^{1/a} \\ &= \tau_0(\xi, \dot{\gamma}) \quad \text{(the flow potential and flow surface)},\end{aligned} \tag{1}$$

$$\dot{\varepsilon}_1 = \dot{\gamma}\frac{\partial \tau}{\partial \sigma_1} = \dot{\gamma}\left[F(\theta)\left(\frac{|\sigma_1|}{\tau}\right)^{a-2}\frac{\sigma_1}{\tau} + H(\theta)\left(\frac{|\sigma_1 - \sigma_2|}{\tau}\right)^{a-2}\frac{(\sigma_1 - \sigma_2)}{\tau}\right],$$

$$\dot{\varepsilon}_2 = \dot{\gamma}\frac{\partial \tau}{\partial \sigma_2} = \dot{\gamma}\left[G(\theta)\left(\frac{|\sigma_2|}{\tau}\right)^{a-2}\frac{\sigma_2}{\tau} - H(\theta)\left(\frac{|\sigma_1 - \sigma_2|}{\tau}\right)^{a-2}\frac{(\sigma_1 - \sigma_2)}{\tau}\right],$$

$$\dot{\varepsilon}_3 = -\dot{\varepsilon}_1 - \dot{\varepsilon}_2,$$

$$\dot{\varepsilon}_{12} = \frac{\dot{\gamma}}{2(\sigma_1 - \sigma_2)}\frac{\partial \tau}{\partial \theta} = \frac{\dot{\gamma}\tau}{a}\left[\frac{F'(\theta)}{2(\sigma_1 - \sigma_2)}\left(\frac{|\sigma_1|}{\tau}\right)^a + \frac{G'(\theta)}{2(\sigma_1 - \sigma_2)}\left(\frac{|\sigma_2|}{\tau}\right)^a + \frac{H'(\theta)}{2(\sigma_1 - \sigma_2)}\left(\frac{|\sigma_1 - \sigma_2|}{\tau}\right)^a\right],$$

$$\dot{\omega}_{12} = \dot{\gamma}\left[-\frac{F'(\theta)\tau}{2a(\sigma_1-\sigma_2)}\left(\frac{|\sigma_1|}{\tau}\right)^a + \frac{G'(\theta)\tau}{2a(\sigma_1-\sigma_2)}\left(\frac{|\sigma_2|}{\tau}\right)^a + \Psi(\theta)\left(\frac{|\sigma_1-\sigma_2|}{\tau}\right)^{a-2}\frac{(\sigma_1-\sigma_2)}{\tau}\right], \quad \text{(the flow rules)} \tag{2}$$

$$\dot{\xi} = \dot{\gamma}\left[F(\theta)\left(\frac{|\sigma_1|}{\tau}\right)^a + G(\theta)\left(\frac{|\sigma_2|}{\tau}\right)^a + Q(,\theta)\left(\frac{|\sigma_1-\sigma_2|}{\tau}\right)^a\right]^{(a-1)/a}, \quad \text{(the evolution law of isotropic hardening)}, \tag{3}$$

$$\tau_0(\xi,\dot{\gamma}) = g_0(\xi+\xi_0)^n\left(\frac{\dot{\gamma}}{\dot{\gamma}_0}\right)^{1/m}, \quad \text{(power}-\text{law strain hardening and rate}-\text{dependence)}, \tag{4}$$

where $\dot{\varepsilon}_1$, $\dot{\varepsilon}_2$, $\dot{\varepsilon}_3$, and $\dot{\varepsilon}_{12}$ are plastic strain rates on the principal axes of stress, $\dot{\omega}_{12}$ is the in-plane plastic spin, τ and $\dot{\gamma}$ are the effective flow stress and its work-conjugate effective plastic strain rate, a (>1) is the stress exponent, $F(\theta)$, $G(\theta)$, $H(\theta)$, $\Psi(\theta)$, and $Q(\theta)$ are five anisotropic material functions of the loading orientation angle, ξ is a certain internal state variable characterizing the isotropic hardening state of the material with its offset value as ξ_0, $\tau_0(\xi,\dot{\gamma})$ is the effective flow strength, g_0 and $\dot{\gamma}_0$ are, respectively, the reference flow strength and the reference strain rate, and n and m are, respectively, strain hardening and rate-sensitivity exponents (with $m\to\infty$ corresponding to the rate-independent limit). Except different names are used for the anisotropic material functions, the above constitutive equations are directly obtained from Eqs. (A.24)–(A.30) by assuming a flow potential with an associated flow rule (Eq. (A.35)), and $c_1(\xi,\dot{\gamma},\theta) = c_2(\xi,\dot{\gamma},\theta) = 1$. The dependence of anisotropic material functions on ξ and $\dot{\gamma}$ is assumed to be negligible.

2.2. Anisotropic material functions and their representations

For orthotropic sheet metals, twofold symmetry exists in each plane along the material symmetry axes. All anisotropic material functions should thus satisfy the following conditions due to the equivalency of the loading orientation angles between θ and $\theta\pm\pi$ (the symmetry of mechanical loading) and θ and $-\theta$ (the orthotropic symmetry of the material)

$$\begin{aligned} &F(\theta) = F(-\theta), \quad F(\theta) = F(\theta\pm\pi), \quad G(\theta) = G(-\theta), \quad G(\theta) = G(\theta\pm\pi),\\ &H(\theta) = H(-\theta), \quad H(\theta) = H(\theta\pm\pi), \quad Q(\theta) = Q(-\theta), \quad Q(\theta) = Q(\theta\pm\pi),\\ &\Psi(\theta) = -\Psi(-\theta), \quad \Psi(\theta) = \Psi(\theta\pm\pi). \end{aligned} \tag{5}$$

These anisotropic material functions need to be defined only for $0\leqslant\theta\leqslant\pi/2$ and each of them may be represented by a cosine or sine Fourier series

$$
\begin{aligned}
F(\theta) &= \sum_{k=0,1,\ldots} F_k \cos 2k\theta = F_0 + F_1 \cos 2\theta + F_2 \cos 4\theta + \cdots, \\
G(\theta) &= \sum_{k=0,1,\ldots} G_k \cos 2k\theta = G_0 + G_1 \cos 2\theta + G_2 \cos 4\theta + \cdots, \\
H(\theta) &= \sum_{k=0,1,\ldots} H_k \cos 2k\theta = H_0 + H_1 \cos 2\theta + H_2 \cos 4\theta + \cdots, \\
Q(\theta) &= \sum_{k=0,1,2\ldots} Q_k \cos 2k\theta = Q_0 + Q_1 \cos 2\theta + Q_2 \cos 4\theta + \cdots, \\
\Psi(\theta) &= \sum_{k=1,2\ldots} \Psi_k \sin 2k\theta = \Psi_1 \sin 2\theta + \Psi_2 \sin 4\theta + \cdots.
\end{aligned} \tag{6}
$$

On the other hand, simple mechanical tests such as uniaxial tension and equal biaxial tension tests are often conducted to evaluate the anisotropic plastic flow behavior of a sheet metal. The relationships between the anisotropic material functions and the experimental measurements are summarized in the following (their derivations are straightforward from Eqs. (1) and (2))

Flow stress under uniaxial tension ($\sigma_1 = \sigma_\theta > 0, \sigma_2 = 0$):

$$\sigma_\theta = \tau_0(\xi, \dot{\gamma})\{F(\theta) + H(\theta)\}^{-1/a}. \tag{7a}$$

Plastic axial strain ratio under uniaxial tension:

$$R_\theta = \left.\frac{\dot{\varepsilon}_2}{\dot{\varepsilon}_3}\right|_{\sigma_\theta} = \frac{H(\theta)}{F(\theta)}. \tag{7b}$$

Plastic shear strain ratio under uniaxial tension:

$$\Gamma_\theta = \left.\frac{\dot{\varepsilon}_{12}}{\dot{\varepsilon}_1}\right|_{\sigma_\theta} = \frac{1}{2a}\,\frac{F'(\theta) + H'(\theta)}{F(\theta) + H(\theta)}. \tag{7c}$$

Plastic spin ratio under uniaxial tension:

$$\Pi_\theta = \left.\frac{\dot{\omega}_{12}}{\dot{\varepsilon}_1}\right|_{\sigma_\theta} = \frac{-F'(\theta)/4 + \Psi(\theta)}{F(\theta) + H(\theta)}. \tag{7d}$$

Flow stress under equal biaxial tension ($\sigma_1 = \sigma_2 = \sigma_B > 0$):

$$\sigma_B = \tau_0(\xi, \dot{\gamma})\{F(0) + G(0)\}^{-1/a}. \tag{7e}$$

Plastic axial strain ratio under equal biaxial tension:

$$\Omega_0 = \left.\frac{\dot{\varepsilon}_2}{\dot{\varepsilon}_1}\right|_{\sigma_B} = \frac{G(0)}{F(0)}. \tag{7f}$$

According to Eq. (A.36), the continuity of the flow surface at equal biaxial loading ($\sigma_1 = \sigma_2 = \sigma_B > 0$) requires

$$F(\theta) + G(\theta) = \left(\frac{\tau}{\sigma_B}\right)^a, \quad \text{so } F'(\theta) + G'(\theta) = 0. \tag{8}$$

Furthermore, if one imposes the more restrictive condition of smoothness on the flow surface under equal biaxial loading (see Eqs. (A.38)–(A.40)), one obtains

$$F(\theta) = G\left(\theta + \frac{\pi}{2}\right) = \left(\frac{1}{2} + \frac{1-\Omega_0}{1+\Omega_0}\frac{\cos 2\theta}{2}\right)\left(\frac{\tau}{\sigma_B}\right)^a. \tag{9}$$

2.3. Some special cases of the proposed anisotropic plastic flow theory

2.3.1. Isotropic plasticity theory by von Mises

With the assumptions of $a = 2$, $F(\theta) = G(\theta) = H(\theta) = Q(\theta) = 1$, the proposed theory becomes identical to that of the von Mises isotropic plasticity flows theory in plane stress condition with $\xi = \gamma$ and

$$\tau = \sqrt{\sigma_1^2 + \sigma_2^2 + (\sigma_1 - \sigma_2)^2} = \sqrt{2}\bar{\sigma}, \tag{10}$$

where $\bar{\sigma}$ is the von Mises effective stress (Hill, 1950; Hosford and Caddell, 1993).

2.3.2. Anisotropic plasticity theory by Hill (1948)

If one prescribes the anisotropic material functions as following ($a = 2$)

$$\begin{aligned} F(\theta) &= \frac{R_{90}+R_0}{2} + \frac{R_{90}-R_0}{2}\cos 2\theta = R_0 \sin^2\theta + R_{90}\cos^2\theta, \\ G(\theta) &= F\left(\theta + \frac{\pi}{2}\right), \quad Q(\theta) = H(\theta), \end{aligned} \tag{11a}$$

$$\begin{aligned} H(\theta) &= \frac{2R_0R_{90} + R_{45}(R_0+R_{90})}{4} + \frac{2R_0R_{90} - R_{45}(R_0+R_{90})}{4}\cos 4\theta \\ &= \frac{1}{2}R_{45}(R_0+R_{90})\sin^2 2\theta + R_0R_{90}\cos^2 2\theta, \end{aligned} \tag{11b}$$

where R_0, R_{45} and R_{90} are the plastic strain ratios measured at 0°, 45°, and 90° from the rolling direction of the sheet metal, respectively, the proposed theory becomes exactly the Hill's (1948) anisotropic plastic flow potential in the plane stress condition expressed in terms of the two principal stresses and the loading orientation angle (Hill, 1948, 1950; Hosford, 1993).

2.3.3. Anisotropic plasticity theories by Hill (1979), Logan and Hosford (1980) and Hosford (1985)

When the principal stress axes coincide with the material symmetry axes, Hill (1979) and Logan and Hosford (1980) proposed a non-quadratic flow potential as

$$f|\sigma_y|^a + g|\sigma_x|^a + h|\sigma_x - \sigma_y|^a = 2\sigma^a, \tag{12}$$

where σ is the effective flow stress, and f, g, and h are material constants. If one sets

$$f = F(0), \quad g = G(0), \quad h = H(0), \quad \text{and} \quad \sigma^a = \tau^a/2, \tag{13}$$

then the flow potential given by Eq. (1) is equivalent to their flow potential. In an attempt to accommodate planar anisotropy and loading without principal stress directions coinciding with material symmetry axes, Hosford (1985) suggested a flow function as

$$R_{\theta+\pi/2}\sigma_1^a + R_\theta\sigma_2^a + R_\theta R_{\theta+\pi/2}(\sigma_1 - \sigma_2)^a = R_{\theta+\pi/2}[1 + R_\theta]\sigma_\theta^a, \tag{14}$$

where σ_θ and R_θ are, respectively, the flow stress and the plastic axial strain ratio in the θ-direction tension test. If one assumes (noting the results given in Eqs. (7a) and (7b))

$$G(\theta) = F(\theta + \pi/2)\frac{H(\theta)}{H(\theta + \pi/2)}, \tag{15}$$

then Eq. (14) is identical to the flow function given by Eq. (1). However, Hosford (1985) did not use the associated flow rule Eq. (2) for the plastic shear strain rate $\dot{\varepsilon}_{12}$. Instead he assumed the principal axes of stress always coincide with those of strain rates so $\dot{\varepsilon}_{12}$ is set to be zero for any loading orientation angle. Possible analytical representations based on a number of uniaxial tension test data σ_θ and R_θ were not discussed at all by Hosford (1985) to describe a flow surface at any loading orientation angle.

2.3.4. Anisotropic plasticity theories by Barlat et al. (1997a,b)

Barlat and colleagues have developed several stress-based anisotropic flow potentials (Yld91, Yld94, Yld96 and Yld2000-2D, etc.) for aluminum sheet metals (Barlat et al., 1991, 1997a,b, 2004). For example, the plane stress versions of their Yld94 (without shear stress) and Yld96 (with shear stress) models can be written separately using their notations as (σ as the effective flow stress)

$$\alpha_x|s_y - s_z|^a + \alpha_y|s_x - s_z|^a + \alpha_z|s_x - s_y|^a = 2\sigma^a, \tag{16a}$$

$$\alpha_1|s_2 - s_3|^a + \alpha_2|s_1 - s_3|^a + \alpha_3|s_1 - s_2|^a = 2\sigma^a, \tag{16b}$$

where (s_x, s_y, s_z) and (s_1, s_2, s_3) are the eigenvalues of the plane stress tensors $\mathbf{s}$ (without and with shear stresses, respectively) modified by a four-order linear operator, and α_x, α_y, and α_z are material anisotropy constants. The parameters α_1, α_2, and α_3 are simply the transformed material anisotropy constants from the principal axes of the anisotropy to the principal axes of $\mathbf{s}$. If the modified plane stress tensor $\mathbf{s}$ is nothing but the deviatoric components of the principal stress tensor defined by σ_1 and σ_2, then the flow potential (Eq. (1)) is equivalent to the special case of either Yld94 or Yld96 model, providing $\sigma^a = \tau^a/2$ and

$$\alpha_x = G(0), \quad \alpha_y = F(0), \quad \alpha_z = H(0), \tag{17a}$$

$$\alpha_1 = G(\theta), \quad \alpha_2 = F(\theta), \quad \alpha_3 = H(\theta). \tag{17b}$$

3. Experimental determinations of anisotropic material functions

3.1. An enhanced evolution law of isotropic hardening

Stress–strain curves obtained in a single equal biaxial tension test and multiple uniaxial tension tests will be used to establish the anisotropic material function $Q(\theta)$ in the evolution law of isotropic hardening given in Eq. (3) so the directional dependence of strain hardening of a sheet metal beyond initial yielding but before

localized necking can be properly described. Using the equal biaxial tensile plastic stress–strain curve as a reference (i.e., the effective flows stress τ is set to be the flow stress σ_B under equal biaxial tension with $\dot{\varepsilon}_B = -\dot{\varepsilon}_3$), each uniaxial tensile plastic stress–strain curve can then be compared at the same isotropic hardening state as (according to Eqs. (7a) and (7e))

$$\frac{\sigma_\theta(\xi,\dot{\gamma})}{\sigma_B(\xi,\dot{\gamma})} = \frac{\sigma_\theta(\varepsilon_\theta,\dot{\varepsilon}_\theta)}{\sigma_B(\varepsilon_B,\dot{\varepsilon}_B)}\bigg|_{(\xi,\dot{\gamma})} = \left[\frac{F(0)+G(0)}{F(\theta)+H(\theta)}\right]^{1/a}. \tag{18}$$

For many sheet metal forming applications under quasi-static loading in ambient environments, the strain rate effects may be negligible and the relevant experimental data are indeed rarely reported. Assuming either $m \to \infty$ or $\dot{\gamma} \equiv \dot{\gamma}_0$ in Eq. (4), the plastic flow stress–strain curves obtained from the equal biaxial tension test and multiple uniaxial tension tests are modeled by a simple power-law in the form of $\sigma(\varepsilon) = \bar{\sigma}(\varepsilon + \bar{\varepsilon})^n$, where n is the strain hardening exponent that is the same for all tests, $\bar{\sigma}$ and $\bar{\varepsilon}$ (about the order of 0.1%) are two material constants that may be different for each test (Graf and Hosford, 1993, 1994). Using such power-law stress–strain curves, the plastic strains in equal biaxial and uniaxial tension tests can be compared as

$$\frac{\varepsilon_\theta(\xi)+\bar{\varepsilon}_\theta(\xi_0)}{\varepsilon_B(\xi)+\bar{\varepsilon}_B(\xi_0)} = \left\{\frac{\bar{\sigma}_B}{\bar{\sigma}_\theta}\left[\frac{F(0)+G(0)}{F(\theta)+H(\theta)}\right]^{1/a}\right\}^{1/n} \quad \text{or}$$

$$\dot{\varepsilon}_\theta(\xi) = \dot{\varepsilon}_B(\xi)\left\{\frac{\bar{\sigma}_B}{\bar{\sigma}_\theta}\left[\frac{F(0)+G(0)}{F(\theta)+H(\theta)}\right]^{1/a}\right\}^{1/n}. \tag{19}$$

On the other hand, there exist direct relations between the isotropic hardening parameter and biaxial and uniaxial plastic tensile strains (using Eqs. (2) and (3))

$$\dot{\xi} = \dot{\varepsilon}_B(\sigma_1=\sigma_2=\sigma_B), \quad \text{and} \quad \dot{\xi} = \dot{\varepsilon}_\theta \frac{[F(\theta)+Q(\theta)]^{(a-1)/a}}{F(\theta)+H(\theta)} \quad (\sigma_1=\sigma_\theta,\sigma_2=0). \tag{20}$$

From Eqs. (19) and (20), one obtains

$$Q(\theta) = [F(\theta)+H(\theta)]^{(a+1/n)/(a-1)}[F(0)+G(0)]^{1/n/(1-a)}\left(\frac{\bar{\sigma}_B}{\bar{\sigma}_\theta}\right)^{a/n/(1-a)} - F(\theta). \tag{21}$$

3.2. The procedure for determining the material functions

Due to its simplicity in laboratory implementation and the high accuracy and reliability of measurements, a sheet metal is commonly investigated by a series of uniaxial tension tests with loading angles at 0°, 45°, and 90° from its rolling direction. Uniaxial stress–strain curves σ_0, σ_{45} and σ_{90} and plastic strain ratios R_0, R_{45}, and R_{90} obtained in these tension tests are then used to determine the

anisotropic material parameters (Hill, 1948, 1950; Graf and Hosford, 1993, 1994; Hosford, 1993; Hosford and Caddell, 1993). To better characterize the planar anisotropy of a sheet metal, uniaxial tension tests with more than three distinct loading orientation angles are used (Gotoh, 1977; Barlat et al., 1997a,b). Occasionally, equal biaxial tension stress–strain curves $\sigma_B(\varepsilon_B)$ by hydraulic bulging tests or by out-of-plane uniaxial compression tests have also been measured for a sheet metal (Pearce, 1968; Woodthorpe and Pearce, 1970; Rata-Eskola, 1979; Young et al., 1981; Vial et al., 1983; Barlat et al., 2004). However, the biaxial plastic strain ratio Ω_0 is only rarely reported in out-of-plane uniaxial compression tests (Bourne and Hill, 1950; Barlat et al., 2004; Tong, 2003). For a given stress exponent a (>1) and a fixed loading orientation angle θ, the four anisotropic material functions $F(\theta)$, $G(\theta)$, $H(\theta)$, and $Q(\theta)$ can then be determined using the following procedure:

(1) Set the stress exponent a to 6 and 8 for BCC and FCC metals, respectively (Hosford, 1993).
(2) Obtain $F(\theta)$ and $G(\theta)$ from Eq. (9) using the flow stress σ_B (with $\tau = \sigma_B$) and the plastic strain ratio Ω_0 under equal biaxial tension (i.e., the smoothness of flow surfaces at equal biaxial loading is assumed).
(3) Determine values of $H(\theta)$ based on the multiple measurements of uniaxial plastic strain ratios R_θ and the known $F(\theta)$ according to Eq. (7b).
(4) Determine values of $Q(\theta)$ based on biaxial and uniaxial stress–strain curves (σ_B, $\bar{\sigma}_\theta$ and n) and the known $F(\theta)$, $G(\theta)$ and $H(\theta)$ using Eq. (21).
(5) Determine the effective flow strength function $\tau_0(\xi, \dot{\gamma})$ in Eq. (4) from the stress–strain curve of the uniaxial tension test along the rolling direction or the equal biaxial tension test (Eqs. (7a) or (7e)):

$$\tau_0(\xi, \dot{\gamma}) = \sigma_0(\varepsilon_0, \dot{\varepsilon}_0)[F(0) + H(0)]^{1/a}, \quad \dot{\xi} = \dot{\varepsilon}_0 \frac{[F(0) + Q(0)]^{(a-1)/a}}{F(0) + H(0)},$$
$$\dot{\gamma} = \dot{\varepsilon}_0 \left\{ \frac{1}{F(0) + H(0)} \right\}^{1/a}, \tag{22}$$

or

$$\tau_0(\xi, \dot{\gamma}) = \sigma_B(\varepsilon_B, \dot{\varepsilon}_B), \quad \dot{\xi} = \dot{\gamma} = \dot{\varepsilon}_B = -\dot{\varepsilon}_3. \tag{23}$$

Because the experimental data are rarely reported on the plastic spin ratio Π_θ under off-axis uniaxial tension (Eq. (7d)), an evaluation of the anisotropic function $\Psi(\theta)$ will be omitted here (for the completeness of the model, it may assume $\Pi_\theta = 0$ so $\Psi(\theta) = F'(\theta)/4/a$). When no experimental data are made available on the biaxial plastic strain ratio Ω_0, one may estimate it from (Tong, 2003)

$$\Omega_0 = \frac{1 + R_0}{1 + R_{90}}. \tag{24}$$

If no equal biaxial tensile stress–strain curve is available, it may be represented by an average of uniaxial tensile stress–strain curves (Wagoner and Wang, 1979; Young et al., 1981)

$$\sigma_B = (\sigma_0 + 2\sigma_{45} + \sigma_{90})/4. \tag{25}$$

To be self-consistent, the material constant $\bar{\varepsilon}_\theta$ in the power-law uniaxial stress–strain curves $\sigma_\theta(\varepsilon_\theta) = \bar{\sigma}_\theta(\varepsilon_\theta + \bar{\varepsilon}_\theta)^n$ should be determined from ($m \to \infty$ or $\dot{\gamma} \equiv \dot{\gamma}_0$ is assumed)

$$\sigma_\theta(0) = \bar{\sigma}_\theta \bar{\varepsilon}_\theta^n \quad \text{or} \quad \bar{\varepsilon}_\theta = \xi_0 \left(\left(\frac{g_0}{\bar{\sigma}_\theta} \right) [F(\theta) + H(\theta)]^{1/a} \right)^{1/n}, \tag{26}$$

where the material constants $\bar{\sigma}_\theta$ and n are determined by a least-square fit of a stress–strain curve at plastic strains of a few percent and above (Graf and Hosford, 1993, 1994).

3.3. Anisotropic plasticity models with various degrees of planar anisotropy

Three anisotropic plasticity models are constructed that correspond to three, five, and seven independent uniaxial tension tests reported for a given sheet metal (the two functions $F(\theta)$ and $G(\theta)$ are given in Eq. (9)):

Anisotropic plasticity Model No. 1:

$$\begin{aligned} H(\theta) &= H_0 + H_1 \cos 2\theta + H_2 \cos 4\theta, \\ Q(\theta) &= Q_0 + Q_1 \cos 2\theta + Q_2 \cos 4\theta. \end{aligned} \tag{27a}$$

Anisotropic plasticity Model No. 2:

$$\begin{aligned} H(\theta) &= H_0 + H_1 \cos 2\theta + H_2 \cos 4\theta + H_3 \cos 6\theta + H_4 \cos 8\theta, \\ Q(\theta) &= Q_0 + Q_1 \cos 2\theta + Q_2 \cos 4\theta + Q_3 \cos 6\theta + Q_4 \cos 8\theta. \end{aligned} \tag{27b}$$

Anisotropic plasticity Model No. 3:

$$\begin{aligned} H(\theta) &= H_0 + H_1 \cos 2\theta + H_2 \cos 4\theta + H_3 \cos 6\theta + H_4 \cos 8\theta + H_5 \cos 10\theta \\ &\quad + H_6 \cos 12\theta, \\ Q(\theta) &= Q_0 + Q_1 \cos 2\theta + Q_2 \cos 4\theta + Q_3 \cos 6\theta + Q_4 \cos 8\theta + Q_5 \cos 10\theta \\ &\quad + Q_6 \cos 12\theta. \end{aligned} \tag{27c}$$

The two material functions at selected loading orientation angles are first determined following the procedure given in Section 3.2, so two sets of linear equations can be solved separately to obtain the Fourier series coefficients of $H(\theta)$ and $Q(\theta)$. For example, the Fourier coefficients in the Model No. 1 are obtained as

$$H_0 = \frac{R_0(F_0+F_1)+R_{45}(F_0-F_1)+2R_{90}F_0}{4}, \quad H_1 = \frac{R_0(F_0+F_1)-R_{45}(F_0-F_1)}{2},$$
$$H_2 = \frac{R_0(F_0+F_1)+R_{45}(F_0-F_1)-2R_{90}F_0}{4}, \tag{28a}$$
$$Q_0 = \frac{Q(\pi/4)}{2}+\frac{Q(0)+Q(\pi/2)}{4}, \quad Q_1 = \frac{Q(0)-Q(\pi/2)}{2},$$
$$Q_2 = -\frac{Q(\pi/4)}{2}+\frac{Q(0)+Q(\pi/2)}{4}. \tag{28b}$$

If $\Omega_0 = R_0/R_{90}$ (which may be called the Hill's (1948) hypothesis on the biaxial plastic strain ratio Ω_0), then $F(\theta)$, $G(\theta)$, and $H(\theta)$ are equivalent to those given in Eqs. (11a) and (11b).

4. Modeling anisotropic plastic flows in orthotropic aluminum sheet metals

4.1. Flow surfaces under fixed loading orientation angles

When a sheet metal is subjected to biaxial tensile loading at a constant loading orientation angle and at a fixed isotropic hardening state, the flow surface projected in (σ_1,σ_2) space can be conveniently generated using the polar coordinates ρ and α (Hill, 1980, 1990)

$$\sigma_1 = \tau_0(\xi,\dot{\gamma})\rho\cos\alpha, \quad \sigma_2 = \tau_0(\xi,\dot{\gamma})\rho\sin\alpha, \quad +\pi/4 \geqslant \alpha \geqslant -\pi/4, \tag{29a}$$
$$\rho|_{(\xi,\dot{\gamma})} = [F(\theta)|\cos\alpha|^a + G(\theta)|\sin\alpha|^a + H(\theta)|\cos\alpha-\sin\alpha|^a]^{-1/a}. \tag{29b}$$

The condition on the angle α of the polar coordinates ($+\pi/4 \geqslant \alpha \geqslant -\pi/4$) is due to the definition of the major principal axis of stress σ_1 ($|\sigma_1| \geqslant |\sigma_2|$). The $+\pi/4 \geqslant \alpha \geqslant 0$ section and the $+\pi/2 \geqslant \alpha \geqslant \pi/4$ section of each flow surface correspond to loading orientation angles of θ and $\theta+\pi/2$, respectively, and they coincide at $\alpha = \pi/4$ (equal biaxial loading). Flow surfaces are often defined either at a given effective plastic strain γ or at a given amount of specific plastic work W_P. Assuming proportional biaxial tensile loading with $\mu = \sigma_2/\sigma_1 = \tan\alpha$, one has (using Eqs. (1) and (3))

$$\dot{\xi} = \dot{\gamma}\left(\frac{F(\theta)+G(\theta)\mu^a+Q(\theta)(1-\mu)^a}{F(\theta)+G(\theta)\mu^a+H(\theta)(1-\mu)^a}\right)^{(a-1)/a}$$
$$\equiv v(\alpha,\theta)\dot{\gamma}, \quad \text{that is } \xi(\gamma;\alpha,\theta) = v(\alpha,\theta)\gamma. \tag{30}$$

Similarly, the plastic work W_P per unit volume under proportional biaxial tension can be related to the isotropic hardening parameter ξ by (using Eqs. (4) and (30))

$$W_P(\xi) = \int_0^\gamma \tau(\xi)\,\mathrm{d}\gamma = \frac{g_0\left[(\xi+\xi_0)^{n+1}-\xi_0^{n+1}\right]}{(1+n)v(\alpha,\theta)},$$
$$\text{or } \xi(W_P) = \left\{\frac{(1+n)v(\alpha,\theta)}{g_0}W_P+\xi_0^{n+1}\right\}^{1/(1+n)}-\xi_0. \tag{31}$$

So the flow surfaces at a constant effective plastic strain γ are given by

$$\sigma_1 = \tau_0(\xi(\gamma;\alpha,\theta),\dot{\gamma})\rho\cos\alpha, \quad \sigma_2 = \tau_0(\xi(\gamma;\alpha,\theta),\dot{\gamma})\rho\sin\alpha, \tag{32a}$$

$$\rho|_{(\gamma,\dot{\gamma})} = \rho|_{(\xi,\dot{\gamma})}\frac{\tau_0(\xi(\gamma;\pi/4,0),\dot{\gamma})}{\tau_0(\xi(\gamma;\alpha,\theta),\dot{\gamma})} = \rho|_{(\xi,\dot{\gamma})}\left(\frac{\xi(\gamma;\pi/4,0)+\xi_0}{\xi(\gamma;\alpha,\theta)+\xi_0}\right)^n \approx \rho|_{(\xi,\dot{\gamma})}\left(\frac{v(\pi/4,0)}{v(\alpha,\theta)}\right)^n. \tag{32b}$$

And the flow surfaces at the same amount of accumulated specific plastic work are given by

$$\sigma_1 = \tau_0(\xi(W_P;\alpha,\theta),\dot{\gamma})\rho\cos\alpha, \quad \sigma_2 = \tau_0(\xi(W_P;\alpha,\theta),\dot{\gamma})\rho\sin\alpha, \tag{33a}$$

$$\rho|_{(W_P,\dot{\gamma})} = \rho|_{(\xi,\dot{\gamma})}\frac{\tau_0(\xi(W_P;\pi/4,0),\dot{\gamma})}{\tau_0(\xi(W_P;\alpha,\theta),\dot{\gamma})} = \rho|_{(\xi,\dot{\gamma})}\left(\frac{\xi(W_P;\pi/4,0)+\xi_0}{\xi(W_P;\alpha,\theta)+\xi_0}\right)^n \approx \rho|_{(\xi,\dot{\gamma})}\left(\frac{v(\pi/4,0)}{v(\alpha,\theta)}\right)^{n/(1+n)}. \tag{33b}$$

The flow surfaces at fixed ξ, γ, and W_P are adjusted so they all coincide under equal biaxial tension.

4.2. Experimental tensile testing data and model parameter identifications of 10 aluminum sheet metals

The three anisotropic plasticity models detailed in Section 3 are used here to describe the plastic flow of a total of 10 commercial aluminum alloy sheet metals. Mechanical testing data of these 10 aluminum alloy sheets have been reported in the literature (see Table 1 for the summary of the 10 aluminum alloys and the cited references). As there are only three uniaxial tension tests (power-law stress–strain curves and plastic strain ratios at 0°, 45°, and 90° from the rolling direction) reported for the first four aluminum sheet metals AA2008-T4, AA6111-T4, AA2036-T4 and

Table 1
List of the references of experimental data on aluminum sheet metals

Materia No.	Alloy designation	No. uniaxial tensile tests	Biaxial test	Model type(s)	References
1	AA2008-T4	3	No	1	Graf and Hosford (1993)
2	AA6111-T4	3	No	1	Graf and Hosford (1994)
3	AA2036-T4	3	No	1	Wagoner and Wang (1979)
4	AA3003-O	3	Yes	1	Vial et al. (1983)
5	AA6XXX-T4	5	No	1,2	Kuwabara et al. (2000)
6	AA6016-T4	7	No	1,2,3	Yoon et al. (1999), Cazacu and Barlat (2001)
7	AA2008-T4	7	No	1,2,3	Barlat et al. (1991)
8	AA2024-T3	7	No	1,2,3	Barlat et al. (1991)
9	AA6022-T4	7	Yes	1,2,3	Barlat et al. (1997b, 2004, 2005)
10	AA2090-T3	7	Yes	1,2,3	Barlat et al. (2004, 2005)

AA3003-O (Graf and Hosford, 1993, 1994; Wagoner and Wang, 1979; and Vial et al., 1983), so only Model No. 1 can be used to describe them. The out-of-plane uniaxial compression test data (equivalent to the in-plane equal-biaxial tension neglecting any hydrostatic pressure effects) are only available for the sheet metal No. 4 (AA3003-O by Vial et al., 1983). No biaxial plastic strain ratios were reported for any of the first four aluminum alloys. There are a total of five uniaxial tension tests (individual power-law stress–strain curves and plastic strain ratios at 0, 22.5°, 45°, 67.5°, and 90° from the rolling direction) but no equal biaxial tension test reported by Kuwabara et al. (2000) for an aluminum sheet metal AA6XXX-T4 (the material No. 5 in Table 1). So both Model No. 1 and Model No. 2 of the new anisotropic plasticity theory can be used to describe its plastic flow behavior. Three uniaxial tensile test data at 0°, 45°, and 90° from the rolling direction are used to determine the material parameters in Model No.1 and all five uniaxial tensile test data at 0°, 22.5°, 45°, 67.5°, and 90° from the rolling direction are used to determine the material parameters in Model No. 2. As the original power-law stress–strain curves given for the first five aluminum sheets use a slightly different power exponent for each test, they have been modified using the same power exponent (averaging from all tests) and by requiring that the new and old power-law stress–strain curves produce the same plastic work at the strain level of 10% (Barlat et al., 1997a,b). The tensile testing data are summarized in Table 2 for both original and modified power-law stress–strain curves of the first five aluminum sheet metals.

Barlat and co-workers have modeled extensively the anisotropic plastic flow of aluminum sheet metals over the years and five of their aluminum sheet metals are selected for this investigation (see Table 1 for details on their published work on these five aluminum alloys). There are a total of seven uniaxial tension tests (normalized yield or flow stresses and plastic strain ratios at 0°, 15°, 30°, 45°, 60°, 75°, and 90° from the rolling direction) reported in their works (Yoon et al., 1999; Barlat et al., 1991, 1997b, 2004) for the five aluminum sheet metals AA6016-T4, AA2008-T4, AA2024-T3, AA6022-T4, and AA2090-T3 (the materials No. 6 to No. 10 in Table 1). The experimental biaxial plastic strain ratio Ω_0 (from an out-of-plane uniaxial compression test) is reported only for one of their aluminum sheet metals AA2090-T3 (Barlat et al., 2004) while biaxial tensile flow stress data are made available for three of their aluminum sheet metals AA6016-T4, AA6022-T4 and AA2090-T3 based on bulge tests. However, no complete power-law type stress–strain curves are reported in the open literature for these five aluminum sheet metals. Except for aluminum sheet metal AA6022-T4 where flow stresses at the equal plastic work at about 0.1 plastic strain are reported (Barlat et al., 1997b), only yield stresses measured by a 0.2% offset strain are given for the rest of the four aluminum sheet metals. A power-law strain hardening exponent $n = 0.25$ is assumed for all of the five aluminum sheet metals and the power-law constants $\bar{\sigma}$ are assumed to be proportional to the uniaxial yield stresses of the four aluminum sheet metals with reported yield stress data (Barlat et al., 2005). The power-law constants $\bar{\sigma}$ for AA6022-T4 are determined based on the reported flow stresses of the equal-plastic work at 10%. Selected normalized yield and flow stresses as well as the power-law constants $\bar{\sigma}$ for the five aluminum sheet metals No. 6 to No. 10 are summarized in Table 2

Table 2
Selected tensile test data on aluminum sheet metals

Aluminum	1	2	3	4	5	6	7	8	9	10
Alloy	2008-T4	6111-T4	2036-T4	3003-O	6xxx-T4	6016-T4	2008-T4	2024-T3	6022-T4	2090-T3
$\bar{\sigma}_0$ (old)	518	548.5	607	195.5	621	1.000	1.000	1.000	0.994	1.000
n (old)	0.264	0.2405	0.226	0.214	0.405	–	–	–	–	–
$\bar{\sigma}_{45}$ (old)	529.5	546	614	187.1	597	0.984	0.944	0.839	0.962	0.811
n (old)	0.2685	0.250	0.246	0.222	0.391	–	–	–	–	–
$\bar{\sigma}_{90}$ (old)	523	541.5	610	183.2	591	0.942	0.902	0.843	0.948	0.910
n (old)	0.264	0.245	0.241	0.215	0.394	–	–	–	–	–
$\bar{\sigma}_0$ (new)	518	550	608.8	195.5	609.1	1.000	1.000	1.000	0.9925	1.000
$\bar{\sigma}_{45}$ (new)	525	544.1	613.7	186.6	601.6	0.984	0.944	0.839	0.9527	0.811
$\bar{\sigma}_{90}$ (new)	523	541.5	609.8	183.2	592.1	0.942	0.902	0.843	0.9354	0.910
n (new)	0.264	0.245	0.240	0.214	0.395	0.250	0.250	0.250	0.250	0.250
R_0	0.580	0.665	0.701	0.655	0.660	0.939	0.852	0.770	0.70	0.21
R_{45}	0.485	0.630	0.752	0.753	0.450	0.386	0.490	1.036	0.48	1.58
R_{90}	0.780	0.785	0.676	0.510	0.570	0.638	0.520	0.658	0.59	0.69
Ω_0	(0.8876)	(0.9328)	(1.0149)	(1.0960)	(1.057)	(1.184)	(1.218)	(1.068)	(1.0692)	0.67
$\bar{\sigma}_B$	(522.75)	(544.9)	(611.5)	176.9	(601.1)	1.000	(1.000)	(1.000)	1.000	1.035

The numbers in the parentheses are estimates using either Eq. (24) or Eq. (25).
The flow stresses are in MPa for the first five alloys but are normalized numbers by $\bar{\sigma}_0$ or $\bar{\sigma}_B$ for other five alloys.

Table 3
Material parameters for selected aluminum sheet metals (Model No. 1, $a = 8$ and $\tau_0 = \sigma_B$)

No.	1	2	3	4	5	6	7	8	9	10
Alloy	2008-T4	6111-T4	2036-T4	3003-O	6xxx-T4	6016-T4	2008-T4	2024-T3	6022-T4	2090-T3
F_0, G_0	0.5000	0.5000	0.5000	0.5000	0.5000	0.5000	0.5000	0.5000	0.5000	0.5000
F_1, $-G_1$	0.0298	0.0174	−0.0037	−0.0229	−0.0139	−0.0421	−0.0492	−0.0163	−0.0167	0.0988
H_0	0.2898	0.3382	0.3601	0.3330	0.2659	0.2905	0.2899	0.4370	0.2808	0.4956
H_1	−0.0298	−0.0174	0.0037	0.0229	0.0139	0.0421	0.0492	0.0163	0.0167	−0.0755
H_2	0.0473	0.0232	−0.0159	−0.0435	0.0409	0.0975	0.0449	−0.0810	0.0408	−0.2944
Q_0	0.1777	0.2416	0.2702	0.5013	0.1722	0.1068	0.0299	0.0104	0.0431	−0.0520
Q_1	−0.0449	0.0110	0.0008	0.1860	0.0434	0.1395	0.1872	0.2237	0.0986	0.0045
Q_2	0.0507	0.0409	−0.0379	−0.0523	0.0525	0.1114	0.0660	0.0483	0.0649	−0.0595
n	0.264	0.245	0.240	0.214	0.395	0.250	0.250	0.250	0.250	0.250
g_0	522.75	544.9	611.5	176.9	601.1	1.000	1.000	1.000	1.000	1.035
ξ_0	0.2%	0.2%	0.2%	0.2%	0.2%	0.2%	0.2%	0.2%	0.2%	0.2%

Table 4
Material parameters for selected aluminum sheet metals (Model No. 2, $a = 8$ and $\tau_0 = \sigma_B$)

Aluminum	5	6	7	8	9	10
Alloy	AA6xxx-T4	AA6016-T4	AA2008-T4	AA2024_T3	AA6022-T4	AA2090-T3
F_0, G_0	0.5000	0.5000	0.5000	0.5000	0.5000	0.5000
F_1, $-G_1$	−0.0139	−0.0421	−0.0492	−0.0163	−0.0167	0.0988
H_0	0.2642	0.2884	0.2943	0.4579	0.2831	0.3477
H_1	0.0051	0.0398	0.0434	0.0133	0.0221	−0.0786
H_2	0.0409	0.0975	0.0449	−0.0810	0.0408	−0.2944
H_3	0.0089	0.0022	0.0058	0.0030	−0.0053	0.0030
H_4	0.0017	0.0021	−0.0044	−0.0209	−0.0023	0.1480
Q_0	0.1672	0.0967	0.0499	0.0133	0.0454	−0.1154
Q_1	0.0313	0.1343	0.1796	0.1810	0.1097	0.0389
Q_2	0.0525	0.1114	0.0660	0.0483	0.0649	−0.0595
Q_3	0.0121	0.0052	0.0075	0.0427	−0.0111	−0.0344
Q_4	0.0050	0.0101	−0.0200	−0.0029	−0.0023	0.0633

(for the uniaxial tensile tests at 0°, 45°, and 90° from the rolling direction only). The anisotropic plasticity Models No. 1 to No. 3 can then be used to describe the flow behaviors of these five aluminum alloy sheets. Three uniaxial tensile test data at 0°, 45°, and 90° from the rolling direction are used to determine the material parameters in Model No. 1, five uniaxial tensile test data at 0°, 30°, 45°, 60°, and 90° from the rolling direction are used to determine the material parameters in Model No. 2, and all seven uniaxial tensile test data are used to determine the material parameters in Model No. 3 for each aluminum alloy according to the procedures given Section 3.

Table 5
Material parameters for selected aluminum sheet metals (Model No. 3, $a = 8$ and $\tau_0 = \sigma_B$)

Aluminum	6	7	8	9	10
Alloy	AA6016-T4	AA2008-T4	AA2024-T3	AA6022-T4	AA2090-T3
F_0, G_0	0.5000	0.5000	0.5000	0.5000	0.5000
F_1, $-G_1$	−0.0421	−0.0492	−0.0163	−0.0167	0.0988
H_0	0.2861	0.2942	0.4538	0.2830	0.3734
H_1	0.0363	0.0490	0.0181	0.0326	−0.0480
H_2	0.0952	0.0448	−0.0850	0.0407	−0.2686
H_3	0.0022	0.0058	0.0030	−0.0053	0.0030
H_4	0.0043	−0.0043	−0.0168	−0.0022	0.1222
H_5	0.0035	−0.0056	−0.0047	−0.0106	−0.0306
H_6	0.0022	0.0001	0.0041	0.0001	−0.0257
Q_0	0.1014	0.0474	0.0038	0.0493	−0.1101
Q_1	0.1317	0.1808	0.1674	0.1195	0.0395
Q_2	0.1161	0.0635	0.0388	0.0688	−0.0542
Q_3	0.0052	0.0075	0.0427	−0.0111	−0.0344
Q_4	0.0053	−0.0175	0.0066	−0.0062	0.0581
Q_5	0.0026	−0.0011	0.0136	−0.0098	−0.0006
Q_6	−0.0048	0.0025	0.0095	−0.0039	−0.0053

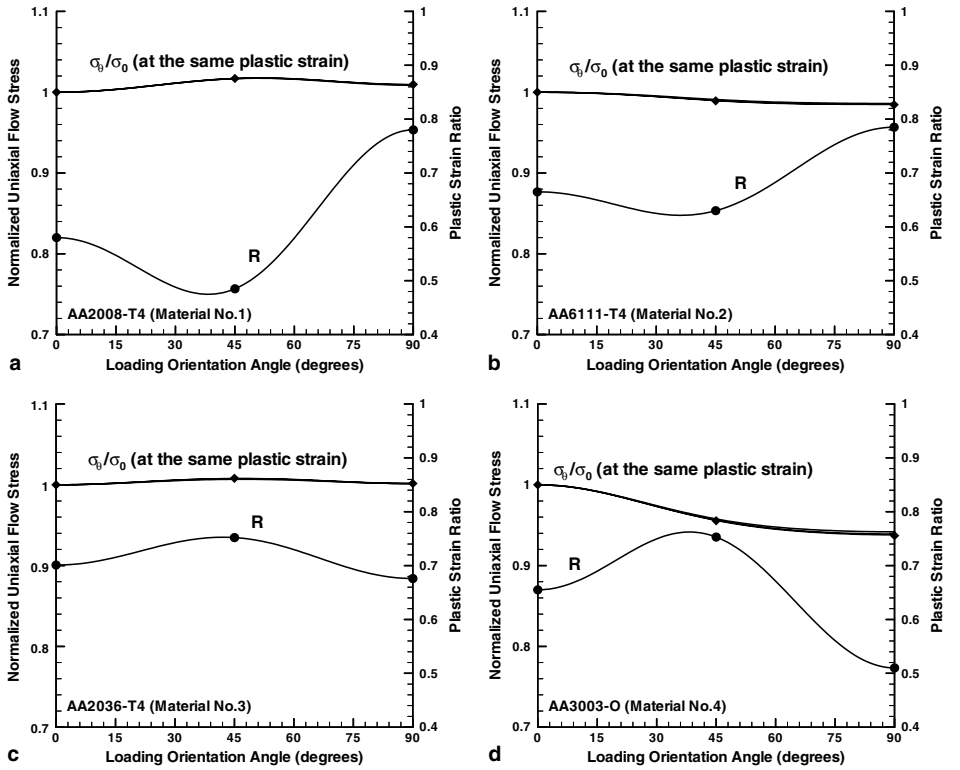

Fig. 1. The predicted directional dependence of flow stress (at the same plastic axial strain) and plastic strain ratio of four aluminum sheet metals under uniaxial tension using the anisotropic plasticity Model No. 1. The reported experimental data (filled symbols) from three uniaxial tension tests at loading orientation angles of 0°, 45°, and 90° are also included for comparison.

If the experimental data are unavailable for the plastic strain ratio and flow stress of any one of the 10 aluminum sheet metals under equal biaxial tension, their values are estimated using Eqs. (24) and (25). Material parameters determined for all of the 10 aluminum sheet metals are given in Table 3 (Model No. 1), Table 4 (Model No. 2), and Table 5 (Model No. 3), respectively. A stress exponent $a = 8$ and the definition of $\tau_0 = \sigma_B$ are used for all aluminum sheet metals.

4.3. Results on modeling the anisotropic plastic flow behavior of 10 aluminum sheet metals

The directional dependence of both flow stress σ_θ (at the same plastic axial strains of 2%, 5% and 10%) and plastic axial strain ratio R_θ under uniaxial tension according to the anisotropic plasticity Model No. 1 is shown in Figs. 1(a)–(d) for the first four aluminum sheet metals (AA2008-T4, AA6111-T4, AA2036-T4, and AA3003-O). The flow stresses at constant uniaxial plastic strains are computed

using Eqs. (7a) and (20b) and normalized by the flow stress σ_0 measured along the rolling direction of each sheet metal. Little difference is observed on the dependence of the flow stress at constant plastic strains on the loading orientation angles when the uniaxial plastic strain is 2% or higher. Also shown in Fig. 1 are the experimental data (the filled symbols) on the flow stress ratio (computed simply from $\bar{\sigma}_\theta/\bar{\sigma}_0$) and the plastic strain ratio. The complete agreement between the experimental measurements and the model description for each sheet metal is expected as the experimental data of both flow stress and plastic strain ratio are used to determine the material parameters in the model.

Similarly, the directional dependence of both flow stress σ_θ (at the same plastic axial strains of 2%, 5% and 10%) and plastic axial strain ratio R_θ under uniaxial tension according to both anisotropic plasticity Models No. 1 (dashed lines) and No. 2 (solid lines) is shown in Fig. 2 for the aluminum sheet metal No. 5 (AA6XXX-T4). Only small difference is observed on the directional dependence of the flow stress between these two models but the Model No. 2 does provide more accurate description of the plastic strain ratio data (because the extra experimental data from the two tensile tests at loading orientation angles of 22.5° and 67.5° are used to establish its material parameters). The directional dependence of both flow stress σ_θ (at the same plastic axial strains of 2%, 5% and 10%) and plastic axial strain ratio R_θ under uniaxial tension given by three anisotropic plasticity Models No. 1 (dashed-dotted lines), No. 2 (dashed lines) and No. 3 (solid lines) is shown in Figs. 3(a)–(e) for the remaining five aluminum sheet metals (AA6016-T4, AA2008-T4, AA2024-T3, AA6022-T4, and AA2090-T3). While the Model No. 1 using only three uniaxial tension tests for its material parameter identification is found to be sufficiently accurate

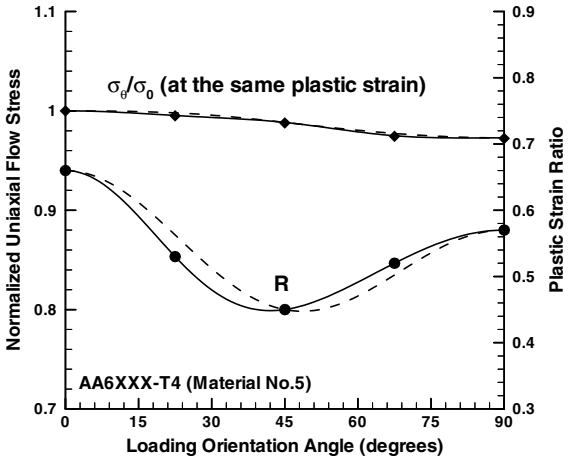

Fig. 2. The predicted directional dependence of flow stress (at the same plastic axial strain) and plastic strain ratio of the aluminum sheet metal AA6XXX-T4 under uniaxial tension using the anisotropic plasticity Models No. 1 (dashed lines) and No. 2 (solid lines). The reported experimental data (filled symbols) from five uniaxial tension tests at loading orientation angles of 0° 22.5°, 45°, 67.5°, and 90° are also included for comparison.

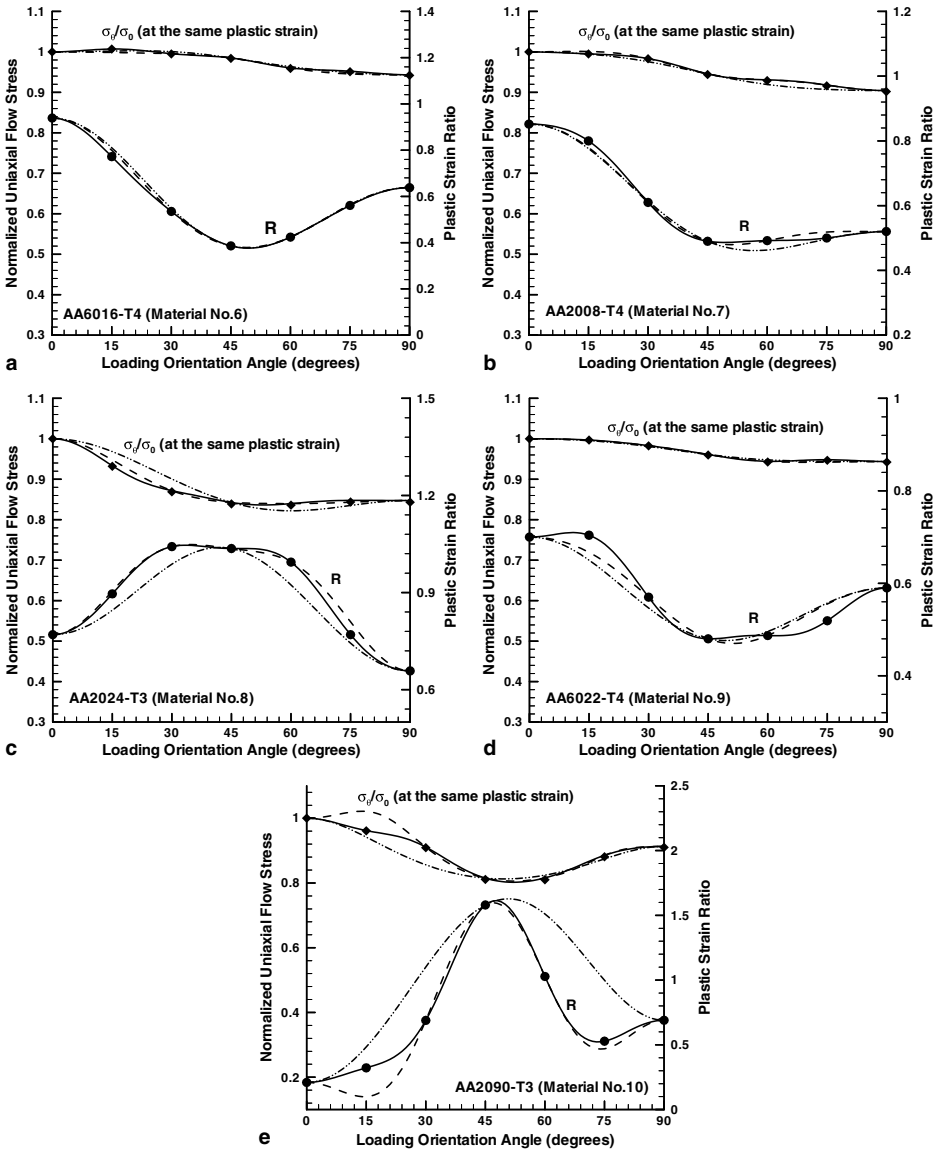

Fig. 3. The predicted directional dependence of flow stress (at the same plastic axial strain) and plastic strain ratio of five aluminum sheet metals under uniaxial tension using the anisotropic plasticity Models No. 1 (dashed-dotted lines), No. 2 (dashed lines), and No. 3 (solid lines). The reported experimental data (filled symbols) from seven uniaxial tension tests at loading orientation angles of 0°, 15°, 30°, 45°, 60°, 75°, and 90° are also included for comparison.

for describing the two aluminum sheet metals AA6016-T4 and AA2008-T4 (No. 6 and No. 7 in Table 1), the model No. 2 (using five uniaxial tension tests for its material parameter identification) is required to adequately capture the planar anisotropy

of aluminum sheet metal AA2024-T3 (see Fig. 3(c)). For the highly textured aluminum sheet metals No. 9 (AA6022-T4) and No. 10 (AA2090-T3), only the Model No. 3 can satisfactorily describe the directional dependence of both flow stress and plastic strain ratio under uniaxial tension. The seven uniaxial tension tests are thus found to be necessary for characterizing these two strongly anisotropic aluminum sheet metals.

The predicted flow surfaces in terms of the biaxial principal tensile stresses (σ_1, σ_2) at a fixed isotropic hardening state ξ and seven fixed loading orientation angles θ are shown in Fig. 4 for two aluminum sheets No. 3 (AA2036-T4) and No. 10 (AA2090-T3). The biaxial flow stresses are normalized by the equal biaxial tension flow stress (recalling the definition of $\tau_0 = \sigma_B$). The seven loading orientation angles are 0°, 15°, 30°, 45°, 60°, 75°, and 90°. Because of the definition of $|\sigma_1| \geqslant |\sigma_2|$ used in this investigation, each flow surface has two sections with $\sigma_1 = \sigma_a$ and $\sigma_1 = \sigma_b$, respectively. All of seven flow surfaces of aluminum sheet metal AA2036-T4 are almost identical, indicating the nearly planar plastic isotropy of this material. On the other hand, the seven flow surfaces of aluminum sheet metal AA2090-T3 are all distinct and they show that its in-plane plastic flow behavior is highly anisotropic. The differences in planar anisotropy of these two aluminum sheet metals are also seen in Figs. 5(a) and (b), where the flow surfaces with a fixed loading orientation angle $\theta = 0$ are compared at the fixed isotropic hardening state ξ (solid line), effective plastic strain γ (dashed line), and accumulated specific plastic work W_P (dash-dotted line). All three types of the flow surfaces are found to be nearly identical for aluminum sheet metal AA2036-T4 but to be clearly distinct for aluminum sheet metal AA2090-T3. The flow surfaces at constant effective plastic strain and accumulated plastic work are very close and stay either outside (AA2036-T4) or inside (AA2090-T3), respectively, the flow surface at the fixed isotropic hardening state defined by ξ.

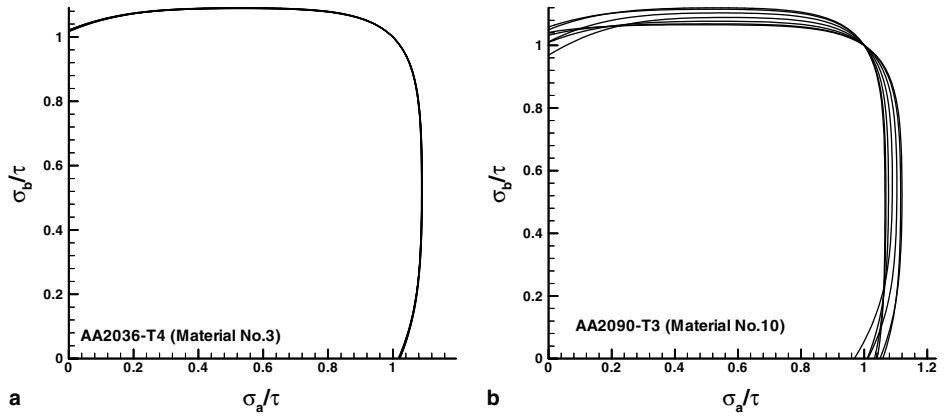

Fig. 4. Predicted biaxial tension flow surfaces of two aluminum sheet metals (a) AA2036-T4 and (b) AA2090-T3 at a fixed isotropic hardening state and seven different loading orientation angles (0°, 15°, 30°, 45°, 60°, 75°, and 90°).

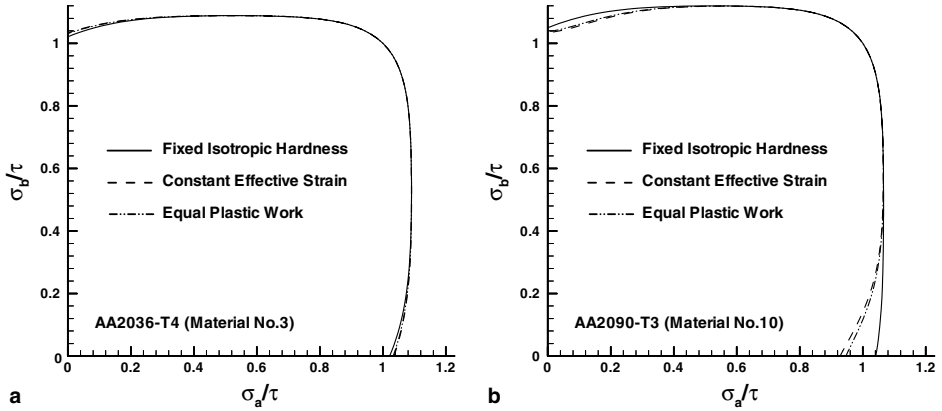

Fig. 5. Comparison of predicted biaxial tension flow surfaces of two aluminum sheet metals (a) AA2036-T4 and (b) AA2090-T3 at the fixed isotropic hardening ξ (solid line), effective plastic strain γ (dashed line), and accumulated plastic work W_P (dash-dotted line). The biaxial tensile loading directions are assumed to coincide with the material symmetry axes (i.e., the loading orientation angles are 0° and 90° for the two sections of each flow surface divided by the equal biaxial tension point).

5. Discussion

A general anisotropic plastic flow theory for sheet metal forming applications should at least account for planar anisotropy and the effect of the in-plane shear stress component, and it should be able to encompass the flow behavior "anomalous" to Hill's (1948) quadratic theory. It is also preferred that the material parameters in the theory have some relevant physical meanings and can be determined by a few simple tests (Barlat, 1987). As a proper evaluation of strongly textured orthotropic sheet metals requires rather extensive experimental data set (Barlat et al., 1991, 2004), the mathematical structure of the theory should be flexible enough to accommodate any additional experimental test data (other than the conventional 0°, 45°, and 90° uniaxial tensile test data) so the accuracy and predictability of the anisotropic plastic flow theory can be improved. Three models with different degrees of planar anisotropy presented in this investigation meet nicely these requirements. These models constructed from a new anisotropic plasticity theory based on effective macroscopic slips have been applied to describe quite satisfactorily the mechanical testing data of selected 10 commercial aluminum sheet metals reported in the literature. These models are also found (Tong et al., 2003) to be adequate to describe the experimental data on the directional dependence of both flow stress and plastic strain ratio under uniaxial tension of other aluminum sheet metals reported by Lademo et al. (1999) and Wu et al. (2003).

Because of many experimental uncertainties and difficulties, the flow stress at small strains (<1%) cannot be reliably and accurately measured for annealed ductile sheet metals under equal biaxial and uniaxial tension (Mellor, 1982). Fortunately, most of sheet metal forming applications (except perhaps springback

and residual stress analyses) involve plastic flows at least a few percent beyond initial yielding. To describe accurately the anisotropic plastic flow behavior of a sheet metal with persistent orthotropy over a wide range of plastic strain (say, from a few percent to 20%–30% or so), proper modeling of both the plastic flow pattern at a fixed isotropic hardening state and the evolution of isotropic hardening under a general plane stress loading is necessary. Most of the efforts in developing the improved anisotropic plasticity models of orthotropic sheet metals in the past have been directed towards formulating ever increasingly sophisticated and complex flow potentials and little or no attention has been paid towards an enhanced description of the evolution of isotropic hardening in sheet metals. The specific form of the resulting anisotropic plastic flow potentials depends strongly on the specific definition of an equivalent isotropic hardening state of a sheet metal after strain hardening under a biaxial loading path. The equivalent isotropic hardening state is often defined in terms of either the equal amount of plastic work per unit volume or the equal effective plastic strain in both isotropic and anisotropic plasticity theories (Hill, 1950; Chakrabarty, 1970; Lubliner, 1990; Khan and Huang, 1995; Barlat et al., 1997a,b, 2004, 2005). The increase in the complexity of anisotropic flow potentials proposed for orthotropic sheet metals in recent years may be in part due to the use of one of these two simple definitions of the equivalent isotropic hardening state. As shown in this investigation, by defining the isotropic hardening state in terms of an internal state variable ξ and its evolution in terms of additional anisotropic functions, a phenomenological anisotropic plasticity model can be developed to describe the complex planar anisotropic plastic flow behavior of a sheet metal rather well over a large range of plastic strain under uniaxial tension and at the same time it is still analytically tractable. For the power-law strain hardening sheet metals modeled, the flow surfaces at the equal effective plastic strain and equal plastic work are rather similar and close but they can be significantly different from the flow surfaces defined at the fixed isotropic hardening state ξ (especially under uniaxial tension), see Fig. 5.

One of the motivations for developing a new anisotropic plasticity theory is to encompass the plastic flow behavior "anomalous" to Hill's quadratic theory (Hill, 1979; Wu et al., 1999; Stoughton, 2002). There are two possible situations that the proposed anisotropic plasticity theory can encompass the "anomalous" behavior. As the ratio of the biaxial flow stress over the uniaxial flow stress at a fixed isotropic hardening state is given by (using Eqs. (7a) and (7e))

$$\frac{\sigma_B(\xi,\dot{\gamma})}{\sigma_0(\xi,\dot{\gamma})}=\frac{\sigma_B(\varepsilon_B,\dot{\varepsilon}_B)}{\sigma_0(\varepsilon_0,\dot{\varepsilon}_0)}\bigg|_{(\xi,\dot{\gamma})}=\left(\frac{1+R_0}{1+\Omega_0}\right)^{1/a}, \tag{34}$$

the new theory may admit the "anomalous" flow if the biaxial plastic strain ratio Ω_0 is about the same or less than the uniaxial plastic strain ratio R_0 (no matter whether or not R_0 is less than 1). The biaxial plastic strain ratio Ω_0 is an independent material parameter required by the theory for its material identification (see Eq. (9)). In comparison, Hill's (1948) quadratic theory predicts that the biaxial plastic strain

ratio Ω_0 must be equal to the ratio R_0/R_{90} and such equality is not universally valid at all for aluminum and copper sheet metals (Barlat et al., 2004; Tong, 2003). More generally, the "anomalous" flow behavior can be interpreted as the isotropic hardening of a sheet metal evolves at two different rates in uniaxial and equal biaxial tensile loading conditions. Comparison of flow stresses under equal biaxial and uniaxial tension is usually made at some accumulated plastic work per unit volume (as it is extremely difficult if not impossible to measure reliably the initial yield stress under equal biaxial tension). In other words, the "anomalous" flow behavior observed in some aluminum sheet metals may be due to the fact that the uniaxial and biaxial flow stresses are compared not at the equivalent isotropic hardening state but at the equal amount of plastic work per unit volume. If the isotropic strain-hardening rate $\dot{\xi}$ under equal biaxial tension is much higher than that under uniaxial tension for the same amount of specific plastic work, the theory can also admit the "anomalous" flow even when Ω_0 is larger than R_0.

The proposed theory also highlights the need for the experimental measurements of both the *plastic shear strain ratio* Γ_θ and the *plastic spin ratio* Π_θ under uniaxial tension. The plastic shear strain ratio Γ_θ can be used to assess the associated flow rule for the shear strain rate component (Tong et al., 2004). The plastic spin ratio Π_θ is needed to fully evaluate the anisotropic material function $\Psi(\theta)$ (so far in this investigation $\Psi(\theta) = F'(\theta)/2$ is assumed for the 10 aluminum sheet metals studied due to lack of any experimental data on their plastic spin ratio Π_θ). A flow rule of plastic spin is an important new feature in the proposed non-quadratic anisotropic plasticity theory (Dafalias, 1985, 2000; McDowell and Moosbrugger, 1992). Its application on modeling the rotation of orthotropic symmetry axes of several sheet metals subjected to off-axis tension (Bunge and Nielsen, 1997; Kim and Yin, 1997) is detailed in a separate investigation (Tong et al., 2004).

It is emphasized that the macroscopic anisotropic plasticity theory that is used to construct the three specific models with various degrees of planar anisotropy in this investigation is a phenomenological one. Such a theory intends to serve as an approximation of a physically based micromechanical polycrystal plasticity theory (Bishop and Hill, 1951a,b; Hosford, 1993) but its simpler mathematical formulation offers great advantages for practical engineering analysis and design in industrial applications. As being discussed in length in the plasticity literature, the key to assess the quality and robustness of a phenomenological plasticity theory is through a series of simple mechanical tests (Hill, 1950; Hosford, 1993). A reasonably well-developed theory is the one that can encompass as many aspects of the experimentally observable anisotropic plastic flow characteristics of a sheet metal as possible. It is contended that such a requirement can serve as a necessary condition and a measure of flexibility and robustness of any good phenomenological anisotropic plasticity theory (although one cannot claim that the theory will provide a reliable description of anisotropic plastic flow behavior under general biaxial loading conditions even if it can provide a complete description of some limited mechanical testing data of a sheet metal). The proposed anisotropic plasticity theory is flexible enough to describe the directional dependence of both flow

stress beyond initial yielding (plastic strain>1%) and plastic strain ratio of a sheet metal under uniaxial tension with any loading orientation angle and to encompass the "anomalous" flow behavior ($\sigma_B \geqslant \sigma_\theta$ at an equal amount of specific plastic work beyond initial yielding when $R_\theta < 1$). At least in this regards, the inclusion of kinematic hardening (Wu et al., 1999; Cao et al., 2000; Wu, 2002; Yao and Cao, 2002) or a non-associated flow potential (Stoughton, 2002) may be unnecessary in an anisotropic plastic theory of sheet metals. If the initial yield stresses can be very reliably measured or if one desires to describe more accurately the directional dependence of flow stresses at small strains (<1%), one may either relax the smoothness condition imposed on the flow surface (Eqs. (9) and (A.38)–(A.40)) or admits one more stress term into the anisotropic plastic flow potential given by Eq. (1). Some of these further refinements are discussed in the separate investigations (Tong, 2003; Tong et al., 2003).

6. Conclusions

Three orthotropic plasticity models with various degrees of planar anisotropy in terms of the principal stresses and a loading orientation angle have been constructed based a recently developed plane stress anisotropic plasticity theory. These three models admitting 8, 12, and 16 anisotropic material parameters, respectively, have been successfully applied to describe the anisotropic plastic flow behavior of selected 10 commercial aluminum sheet metals. The proposed models are analytical tractable and their material parameters can be easily evaluated experimentally by a single equal biaxial tension test and three, five, and seven uniaxial tension tests, respectively. An enhanced evolution law of isotropic hardening other than the effective strain or equivalent plastic work in the theory provides greater flexibility so the entire power-law uniaxial stress–strain curves beyond initial yielding (>1% plastic strain) under various loading orientation angles can be adequately described. Experimental measurements of both *biaxial* plastic strain ratio and plastic *shear* strain ratio are needed for an accurate and thorough self-consistent evaluation of these orthotropic plastic flow models.

Acknowledgments

The work reported here is part of the on-going sheet metal plasticity research effort at Yale University supported in part by the National Science Foundation (Grant No. CMS-973397, Program Director: Dr. K. Chong). Additional financial and technical supports from Alcoa Technical Center (H. Weiland) and Olin Metals Research Labs (F. N. Mandigo) are gratefully acknowledged. The author is indebted to Dr. F. Barlat (Alcoa Technical Center) for sharing their excellent work (Barlat et al., 2004, 2005) and for suggestions on modeling their aluminum alloys. The author is very grateful of valuable comments of anonymous reviewers that have helped a great deal in improving the presentation of the paper.

Appendix A. Anisotropic plastic flows by macroscopic slips

In this appendix, the deformation kinematics and constituvtive relations of a new anisotropic plastic flow theory for an orthotropic polycrystalline sheet metal are re-derived in detail by considering the planar anisotropic plastic flow in terms of several discrete equivalent planar macroscopic double slips (Tong, 2005).

A.1. Deformation kinematics

The formulation of the macroscopic slip plasticity theory follows closely that of continuum crystallographic slips in single crystals (Bishop and Hill, 1951a,b; Rice, 1971; Bassani, 1994; Khan and Huang, 1995). However, each macroscopic slip is assumed to occur uniformly throughout a macroscopic material element and to be the average of crystallographic slips of representative polycrystalline grain aggregates, see Fig. 6. The velocity gradient $\mathbf{L}$ for elasto-plastic deformations can be written as the sum of the symmetric rate of deformation $\mathbf{D}$ and anti-symmetric spin $\mathbf{W}$:

$$\mathbf{L} = \mathbf{D} + \mathbf{W}. \tag{A.1}$$

The rate of deformation and spin tensors can be decomposed into a lattice part (superscript *) and a plastic part (superscript p) as

$$\mathbf{D} = \mathbf{D}^{*} + \mathbf{D}^{\mathrm{p}}, \quad \mathbf{W} = \mathbf{W}^{*} + \mathbf{W}^{\mathrm{p}}. \tag{A.2}$$

The elastic rate of deformation $\mathbf{D}^*$ is negligible for metals and alloys, and the plastic part of the above equations can be represented by shear strains associated with macroscopic *slip modes*:

$$\mathbf{D} \approx \mathbf{D}^{\mathrm{p}} = \sum_{n=1}^{N} \dot{\gamma}_n \mathbf{P}_n, \quad \mathbf{W}^{\mathrm{p}} = \sum_{n=1}^{N} \dot{\gamma}_n \mathbf{Q}_n, \tag{A.3}$$

where $\dot{\gamma}_n$ is the absolute value of the rate of change of integrated shear strain for the nth slip mode, and N is the total number of activated slip modes. Each macroscopic slip mode is composed of a slip direction and a slip plane. The tensors $\mathbf{P}_n$ and $\mathbf{Q}_n$ for the nth slip mode are defined by

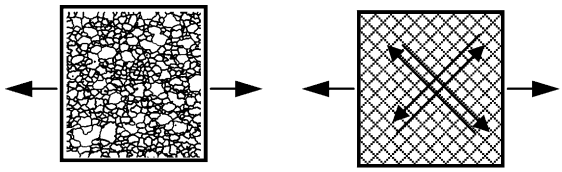

(a) a polycrystal *(b) the macroscopic slip mode*

Fig. 6. Schematic of a macroscopic double slip mode in a polycrystalline sheet metal under tension: (a) a polycrystal, (b) the macroscopic slip mode.

$$\mathbf{P}_n = \operatorname{sym}\mathbf{T}_n = \frac{1}{2}(\mathbf{s}_n \otimes \mathbf{m}_n + \mathbf{m}_n \otimes \mathbf{s}_n), \quad \mathbf{Q}_n = \operatorname{skew}\mathbf{T}_n$$
$$= \frac{1}{2}(\mathbf{s}_n \otimes \mathbf{m}_n - \mathbf{m}_n \otimes \mathbf{s}_n), \tag{A.4}$$

where the Schmid tensor $\mathbf{T}_n$ is defined by $\mathbf{T}_n = \mathbf{s}_n \otimes \mathbf{m}_n$, and unit vectors $\mathbf{s}_n$ and $\mathbf{m}_n$ are the slip direction and normal to the slip plane associated with the nth slip mode in the deformed configuration, respectively. As we consider plastic flows of a polycrystalline metal, the slip modes here refer to *macroscopic* shearing deformation modes averaged from the crystallographic slip systems of a set of grains that constitute the representative polycrystalline material element. In general, there are an infinite number of possible slip modes in a polycrystalline sample. However, only a small fraction of these macroscopic slip modes may be activated, depending on the driving force, the slip resistance on each macroscopic slip plane, and kinematic constraints. As the typical volume preserving condition in a plastically deforming solid is automatically satisfied in the above slip equations, an arbitrary plastic flow is *kinematically admissible* if five or more independent macroscopic slips are activated (Bishop and Hill, 1951a,b; Hosford, 1993). For arbitrary planar plastic flows in which no out-of-plane shearing is allowed, a minimum number of three independent macroscopic slips are required.

A.2. Slip conditions

Activation of selected macroscopic slip modes can be prescribed by certain slip conditions. The driving force to activate a slip mode is the resolved shear stress τ_n on the corresponding slip plane in the current configuration, which can be obtained by $\tau_n = \mathbf{P}_n{:}\boldsymbol{\sigma}$, where $\boldsymbol{\sigma}$ is the Cauchy stress tensor. The condition for a macroscopic slip may be of the following functional form:

$$f_n(\tau_1, \tau_2, \ldots, \tau_N) = 0. \tag{A.5}$$

The Schmid law commonly used for activating a crystallographic slip in a single crystal (Bassani, 1994; Khan and Huang, 1995) can be regarded as one of possible macroscopic slip conditions.

A.3. Rate-dependent slip laws

To complete the description of the plastic flow in terms of macroscopic slips, a constitutive equation on the individual slip rate $\dot{\gamma}_\alpha$ is required in terms of the driving forces, namely,

$$\dot{\gamma}_n = q_n(\tau_1, \tau_2, \ldots, \tau_N). \tag{A.6}$$

Again, many forms of slip rate equations proposed for crystallographic slips in single crystals may be possible choices for the macroscopic slip law as well. Invoking the familiar concept of flow potential used in many phenomenological theories of plasticity, the slip law may also be written as

$$\dot{\gamma}_n = \lambda \frac{\partial g(\tau_1, \tau_2, \ldots, \tau_N)}{\partial \tau_n}, \tag{A.7}$$

where $g(\tau_1, \tau_2, \ldots, \tau_N)$ is a stress-based slip potential and λ is a parameter depending on the external loading and prior deformation history. Isotropic and anisotropic strain hardening behaviors including Bauschinger effects can also be considered by prescribing some scalar and tensor valued internal state variables and their evolution equations in addition to the above slip laws (Rice, 1971; Lubliner, 1990; Karafillis and Boyce, 1993; Khan and Huang, 1995; Wu et al., 1999).

A.4. Plane stress constitutive equations in terms of macroscopic slips

As shown in Fig. 7, a polycrystalline material element may be defined by a Cartesian material texture coordinate system in terms of the rolling direction (x), the transverse direction (y) and the normal direction (z) of an orthotropic sheet metal. A plane stress state commonly exists in a sheet metal undergoing in-plane drawing, shearing and stretching operations and it can be simply described by the two principal stress components in the x–y plane, the major principal stress σ_1 and the minor principal stress σ_2, with the out-of-plane normal stress $\sigma_3 = 0$,

$$\boldsymbol{\sigma} = \begin{pmatrix} \sigma_1 & & \\ & \sigma_2 & \\ & & 0 \end{pmatrix}, \quad |\sigma_1| \geqslant |\sigma_2|, \tag{A.8}$$

and a *loading orientation angle* θ which is defined as the angle between the direction of the major principal stress component σ_1 and the rolling direction of the sheet metal. When $\sigma_1 = \sigma_2$, the principal axes of stress are set to coincide with the principal axes of strain rates, so the loading orientation angle is zero. The

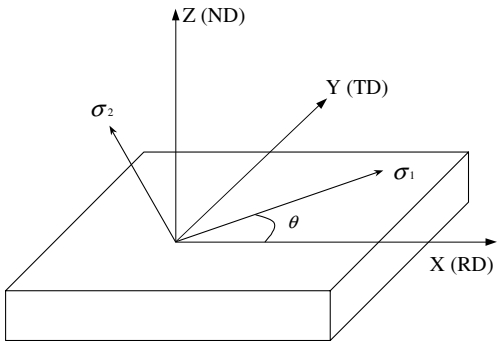

Fig. 7. The sheet metal material texture coordinate system is defined in terms of the rolling direction (x), the transverse direction (y) and the normal direction (z). The principal stress loading direction is defined by the loading orientation angle θ ($|\sigma_1| \geqslant |\sigma_2|$).

tensile normal stresses are defined to be positive and compressive normal stresses are defined to be negative. The planar plastic flow may be conveniently described by discrete macroscopic double slips on three planes defined by the principal stress directions, see Fig. 8. There are a total of six macroscopic slip modes (shown as dashed lines in Fig. 8) that may be activated with two slip modes on each of these three planes 1–3, 2–3, and 1–2. For planar plastic flows in an orthotropic sheet metal under plane stress, both out-of-plane shear strain rates are zero ($\dot{\varepsilon}_{13} = \dot{\varepsilon}_{23} = 0$). So the two slip modes on both planes 1–3 and 2–3 are symmetric (both the angles of the slip direction from the principal loading

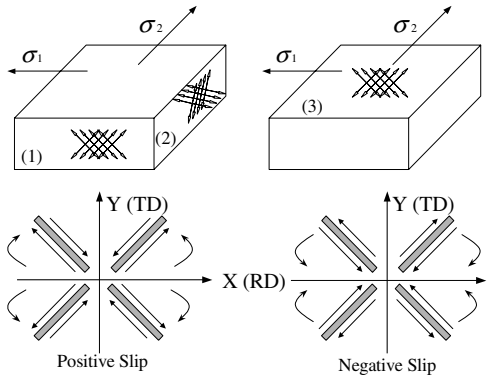

(1) Schematic of three macroscopic slip planes.

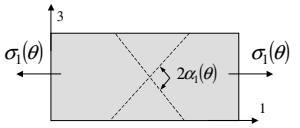

(a) Symmetric Double Slip Mode No.1

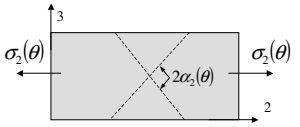

(b) Symmetric Double Slip Mode No.2

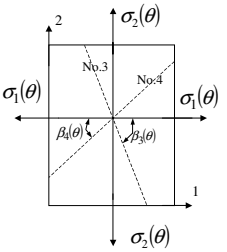

(c) In-Plane Slip Modes No.3 and No.4

(2) Definitions of angles of the four independent slip planes.

Fig. 8. Three macroscopic double slip modes defined in the principal stress directions. The two out-of-plane shearing modes No. 1 and No. 2 are symmetric double slips and they are activated by the resolved shear stresses τ_1^* and τ_2^*, respectively. The double slips of the in-plane shearing modes No. 3 and No. 4 activated by the resolved shear stresses τ_3^* and τ_4^* are in general non-symmetric. Also shown in the figure are four equivalent slip planes of the in-plane shearing mode and two possible slip directions (positive and negative) on each slip plane with respect to the fixed sheet metal orthotropic symmetry axes.

directions and the slip rate magnitudes are identical). The two slip modes in the plane 1–2 are in general not symmetric due to planar anisotropy of the material. One can write out the slip direction and slip plane normal for each of the six slip modes as (four of them may be completely independent)

$$\begin{aligned}
&\mathbf{s}_{1a} = \mathrm{sgn}(\sigma_1)(-\cos\alpha_1\cos\delta_1, \sin\delta_1, \sin\alpha_1\cos\delta_1), \quad \mathbf{m}_{1a} = (-\sin\alpha_1, 0, -\cos\alpha_1),\\
&\mathbf{s}_{1b} = \mathrm{sgn}(\sigma_1)(-\cos\alpha_1\cos\delta_1, \sin\delta_1, -\sin\alpha_1\cos\delta_1), \quad \mathbf{m}_{1b} = (-\sin\alpha_1, 0, \cos\alpha_1),\\
&\mathbf{s}_{2a} = \mathrm{sgn}(\sigma_2)(\sin\delta_2, -\cos\alpha_2\cos\delta_2, \sin\alpha_2\cos\delta_2), \quad \mathbf{m}_{2a} = (0, -\sin\alpha_2, -\cos\alpha_2),\\
&\mathbf{s}_{1b} = \mathrm{sgn}(\sigma_2)(-\cos\alpha_1\cos\delta_2, \sin\delta_2, -\sin\alpha_1\cos\delta_2), \quad \mathbf{m}_{1b} = (-\sin\alpha_1, 0, \cos\alpha_1),\\
&\mathbf{s}_3 = (-\cos\beta_3, \sin\beta_3, 0), \quad \mathbf{m}_3 = (-\sin\beta_3, -\cos\beta_3, 0),\\
&\mathbf{s}_4 = (-\cos\beta_4, -\sin\beta_4, 0), \quad \mathbf{m}_4 = (-\sin\beta_4, \cos\beta_4, 0),
\end{aligned} \tag{A.9}$$

where $\alpha_1, \alpha_2, \beta_3$ and β_4 are the actual angles (all are with the range from 0 to $\pi/2$) between the slip planes and the principal loading directions defined in Fig. 8 for the four independent slip modes and δ_1 and *delta*$_2$ are the offset angles of the slip directions of the two out-of-plane shear modes due to material anisotropy (all six angles are assumed to depend in general on the external loading condition, i.e., on both the loading orientation angle θ and the principal stresses). The symmetric rate of plastic deformation $\mathbf{D}^{\mathrm{p}}$ and anti-symmetric plastic spin $\mathbf{W}^{\mathrm{p}}$ can then be obtained via Eqs. (A.3), (A.4) and (A.9)

$$\begin{aligned}
\mathbf{D}^{\mathrm{p}} &= \begin{pmatrix} \dot\varepsilon_1 & \dot\varepsilon_{12} & 0 \\ \dot\varepsilon_{21} & \dot\varepsilon_2 & 0 \\ 0 & 0 & \dot\varepsilon_3 \end{pmatrix}\\
&= \begin{pmatrix} \frac{\dot\gamma_1^*\sigma_1\sin 2\alpha_1}{|\sigma_1|} + \frac{\dot\gamma_3^*\sin 2\beta_3 + \dot\gamma_4^*\sin 2\beta_4}{2} & -\frac{\dot\gamma_1^*\sigma_1\sin\alpha_1\sin\delta_1}{|\sigma_1|} - \frac{\dot\gamma_2^*\sigma_2\sin\alpha_2\sin\delta_2}{|\sigma_2|} + \frac{\dot\gamma_3^*\cos 2\beta_3 - \dot\gamma_4^*\cos 2\beta_4}{2} & 0 \\ \dot\varepsilon_{12} & \frac{\dot\gamma_2^*\sigma_2\sin 2\alpha_2}{|\sigma_2|} - \frac{\dot\gamma_3^*\sin 2\beta_3 + \dot\gamma_4^*\sin 2\beta_4}{2} & 0 \\ 0 & 0 & -\dot\varepsilon_1 - \dot\varepsilon_2 \end{pmatrix},
\end{aligned} \tag{A.10}$$

$$\mathbf{W}^{\mathrm{p}} = \begin{pmatrix} \dot\omega_1 & \dot\omega_{12} & \dot\omega_{13} \\ \dot\omega_{21} & \dot\omega_{22} & \dot\omega_{23} \\ \dot\omega_{31} & \dot\omega_{32} & \dot\omega_{33} \end{pmatrix} = \begin{pmatrix} 0 & \frac{\dot\gamma_1^*\sigma_1\sin\alpha_1\sin\delta_1}{|\sigma_1|} - \frac{\dot\gamma_2^*\sigma_2\sin\alpha_2\sin\delta_2}{|sigma_2|} + \frac{\dot\gamma_3^* - \dot\gamma_4^*}{2} & 0 \\ -\dot\omega_{12} & 0 & 0 \\ 0 & 0 & 0 \end{pmatrix}, \tag{A.11}$$

where $\dot\gamma_1^*$, $\dot\gamma_2^*$, $\dot\gamma_3^*$ and $\dot\gamma_4^*$ are the slip rates (all are non-negative in values) on each of the four independent slip modes defined in Fig. 8. The resolved shear stresses on the macroscopic slip planes along the slip directions with respect to the principal loading directions are given as (all are non-negative in values)

$$\begin{aligned}
\tau_1^* &= \operatorname{sgn}\{\sigma_1\}\frac{\sigma_1}{2}\sin 2\alpha_1\cos\delta_1 = \tau_1\sin 2\alpha_1\cos\delta_1,\\
\tau_2^* &= \operatorname{sgn}\{\sigma_2\}\frac{\sigma_2}{2}\sin 2\alpha_2\cos\delta_2 = \tau_2\sin 2\alpha_2\cos\delta_2,\\
\tau_3^* &= \frac{\sigma_1-\sigma_2}{2}\sin 2\beta_3 = \tau_3\sin 2\beta_3,\\
\tau_4^* &= \frac{\sigma_1-\sigma_2}{2}\sin 2\beta_4 = \tau_4\sin 2\beta_4,\\
&\text{with } \tau_1 = \operatorname{sgn}\{\sigma_1\}\frac{\sigma_1}{2},\ \tau_2 = \operatorname{sgn}\{\sigma_2\}\frac{\sigma_2}{2},\ \tau_3 = \tau_4 = \frac{\sigma_1-\sigma_2}{2},
\end{aligned} \tag{A.12}$$

where τ_1, τ_2, and $\tau_3 = \tau_4$ are the *maximum* resolved shear stresses on the three planes that double slip modes occur, Similar to Eq. (A.12), the non-zero terms in the above Eqs. (A.10) and (A.11) can be rewritten out as

$$\begin{aligned}
&\dot\varepsilon_1 = \operatorname{sgn}(\sigma_1)\dot\gamma_1 + \frac{1}{2}\dot\gamma_3 + \frac{1}{2}\dot\gamma_4, \quad \dot\varepsilon_2 = \operatorname{sgn}(\sigma_2)\dot\gamma_2 - \frac{1}{2}\dot\gamma_3 - \frac{1}{2}\dot\gamma_4,\\
&\dot\varepsilon_3 = -\operatorname{sgn}(\sigma_1)\dot\gamma_1 - \operatorname{sgn}(\sigma_2)\dot\gamma_2,\\
&\dot\varepsilon_{12} = -\operatorname{sgn}(\sigma_1)\frac{\dot\gamma_1\sin\delta_1}{2\cos\alpha_1} - \operatorname{sgn}(\sigma_2)\frac{\dot\gamma_2\sin\delta_2}{2\cos\alpha_2} + \frac{\dot\gamma_3\cos 2\beta_3}{2\sin 2\beta_3} - \frac{\dot\gamma_4\cos 2\beta_4}{2\sin 2\beta_4},\\
&\dot\omega_{12} = \operatorname{sgn}(\sigma_1)\dot\gamma_1\frac{\sin\delta_1}{2\cos\alpha_1} - \operatorname{sgn}(\sigma_2)\frac{\dot\gamma_2\sin\delta_2}{2\cos\alpha_2} + \frac{\dot\gamma_3}{2\sin 2\beta_3} - \frac{\dot\gamma_4}{2\sin 2\beta_4},\\
&\text{with } \dot\gamma_1 = \dot\gamma_1^*\sin 2\alpha_1,\ \dot\gamma_2 = \dot\gamma_2^*\sin 2\alpha_2,\ \dot\gamma_3 = \dot\gamma_3^*\sin 2\beta_3,\ \dot\gamma_4 = \dot\gamma_4^*\sin 2\beta_4,
\end{aligned} \tag{A.13}$$

where $\dot\gamma_1$, $\dot\gamma_2$, $\dot\gamma_3$ and $\dot\gamma_4$ can be regarded as the equivalent slip rates of macroscopic slip modes activated by the maximum resolved shear stresses τ_1, τ_2, τ_3, and τ_4 with the slip directions at the angles of 45° from the principal loading directions. The positive and negative axial strain rates represent extension and contraction of the sheet metal sample in the principal loading directions, respectively. The first two double-slip modes are out-of-plane shearing deformation modes on two orthogonal through-thickness planes and they are always symmetrical for *planar* plastic flow of orthotropic sheet metals (so only single slip rate $\dot\gamma_1$ or $\dot\gamma_2$ is prescribed for each double-slip mode). The third one is the in-plane shearing deformation mode and in general it is non-symmetrical due to the planar anisotropy of sheet metals (so two independent slip rates $\dot\gamma_3$ and $\dot\gamma_4$ are prescribed). These three sets of double-slip modes with *four* independent slip systems (out of a total of six slip systems) are *kinematically sufficient* for representing any planar plastic flows in terms of the principal loading directions (which are not coincided with the principal straining directions as in general $\dot\varepsilon_{12} \neq 0$!).

A power-law viscous shearing flow model is assumed for each slip mode

$$\dot\gamma_1^* = \frac{\left[\tau_1^*\right]^{a-1}}{\eta_1^*}, \quad \dot\gamma_2^* = \frac{\left[\tau_2^*\right]^{a-1}}{\eta_2^*}, \quad \dot\gamma_3^* = \frac{\left[\tau_3^*\right]^{a-1}}{\kappa_3^*}, \quad \dot\gamma_4 = \frac{\left[\tau_4^*\right]^{a-1}}{\kappa_4^*}, \tag{A.14}$$

where $a-1$ (>0) is the stress exponent constant for the viscous shearing, η^* and κ^* are viscosity coefficients of the out-of-plane and in-plane macroscopic shearing modes, respectively. Both viscosity coefficients are assumed to be positive-valued functions of a certain internal state variable ξ characterizing the isotropic hardening state of the material and the effective shear strain rate $\dot{\gamma}^*$ characterizing the current loading of the deforming polycrystalline element (Rice, 1971; Lubliner, 1990; Khan and Huang, 1995). All viscosity coefficients may depend on both the loading orientation angle θ and the principal stresses. The above power-law viscous shearing flow model for each slip mode can be rewritten as

$$\begin{aligned}
&\dot{\gamma}_1 = \frac{\tau_1^{a-1}}{\tilde{\eta}_1}, \quad \dot{\gamma}_2 = \frac{\tau_2^{a-1}}{\tilde{\eta}_2}, \quad \dot{\gamma}_3 = \frac{\tau_3^{a-1}}{\tilde{\kappa}_3}, \quad \dot{\gamma}_4 = \frac{\tau_4^{a-1}}{\tilde{\kappa}_4},\\
&\tilde{\eta}_1 = \frac{\eta_1^*}{(\sin 2\alpha_1)^a(\cos\delta_1)^{a-1}}, \quad \tilde{\eta}_2 = \frac{\eta_2^*}{(\sin 2\alpha_2)^a(\cos\delta_2)^{a-1}},\\
&\tilde{\kappa}_3 = \frac{\kappa_3^*}{(\sin 2\beta_3)^a}, \quad \tilde{\kappa}_4 = \frac{\kappa_4^*}{(\sin 2\beta_4)^a}.
\end{aligned} \tag{A.15}$$

As shown in Eqs. (A.8)–(A.15), the planar plastic flow in a sheet metal under plane stress may be completely described by the four *equivalent* slip modes occurring at the angles of 45° from the principal loading directions (except the in-plane shearing strain rate $\dot{\varepsilon}_{12}$ where the additional knowledge on δ_1, δ_2, β_3 and β_4 is needed). For simplicity, only the four equivalent slip rates $\dot{\gamma}_1$, $\dot{\gamma}_2$, $\dot{\gamma}_3$ and $\dot{\gamma}_4$ and their driving forces on each slip mode τ_1, τ_2, τ_3, and τ_4 will be used to continue the formulating of the macroscopic slip model. The effective shear stress τ and its conjugate effective shear strain rate $\dot{\gamma}$ are defined as usual by assuming the equivalency of the plastic work rate per unit volume $\dot{W}^{\mathrm{p}}$ between an effective symmetrical double slip and the four macroscopic slips, namely,

$$\dot{W}^{\mathrm{p}} = 2\tau\dot{\gamma} = 2\tau_1\dot{\gamma}_1 + 2\tau_2\dot{\gamma}_2 + \tau_3\dot{\gamma}_3 + \tau_4\dot{\gamma}_4. \tag{A.16}$$

The same nonlinear viscous flow model is *assumed* for the effective shear stress τ and the effective shear strain rate $\dot{\gamma}$

$$\dot{\gamma}(\xi,\tau) = \frac{\tau^{a-1}}{\bar{\eta}(\xi,\tau)} \quad \text{or} \quad \tau(\xi,\dot{\gamma})^{a-1} = \bar{\eta}(\xi,\dot{\gamma})\dot{\gamma}, \tag{A.17}$$

where $\bar{\eta}$ is the effective viscosity coefficient of the polycrystalline sheet metal. When the viscosity coefficients $\tilde{\eta}$ and $\tilde{\kappa}$ are normalized by the effective viscosity coefficient $\bar{\eta}$ as η and κ, respectively. Eq. (A.15) may be rewritten as

$$\begin{aligned}
&\dot{\gamma}_1 = \frac{\dot{\gamma}}{\eta_1}\left(\frac{\tau_1}{\tau}\right)^{a-1}, \quad \dot{\gamma}_2 = \frac{\dot{\gamma}}{\eta_2}\left(\frac{\tau_2}{\tau}\right)^{a-1}, \quad \dot{\gamma}_3 = \frac{\dot{\gamma}}{\kappa_3}\left(\frac{\tau_3}{\tau}\right)^{a-1},\\
&\dot{\gamma}_4 = \frac{\dot{\gamma}}{\kappa_4}\left(\frac{\tau_4}{\tau}\right)^{a-1}.
\end{aligned} \tag{A.18}$$

Eqs. (A.16) and (A.17) lead to the following expressions for the effective shear strain rate and effective shear stress, respectively

$$\dot{\gamma}^{\frac{a}{a-1}} = \eta_1^{\frac{1}{a-1}}\dot{\gamma}_1^{\frac{a}{a-1}} + \eta_2^{\frac{1}{a-1}}\dot{\gamma}_2^{\frac{a}{a-1}} + \frac{1}{2}\kappa_3^{\frac{1}{a-1}}\dot{\gamma}_3^{\frac{a}{a-1}} + \frac{1}{2}\kappa_4^{\frac{1}{a-1}}\dot{\gamma}_4^{\frac{a}{a-1}} \tag{A.19}$$

and

$$\tau = \left[\frac{\tau_1^a}{\eta_1} + \frac{\tau_2^a}{\eta_2} + \frac{\tau_3^a}{2\kappa_3} + \frac{\tau_4^a}{2\kappa_4}\right]^{\frac{1}{a}}. \tag{A.20}$$

The evolution for the isotropic hardening parameter ξ is generally characterized by a rate-type kinetic equation under plastic loading in the form of (Lubliner, 1990)

$$\dot{\xi} = \dot{\xi}(\xi, \tau_1, \tau_2, \tau_3, \tau_4) = \dot{\xi}(\xi, \dot{\gamma}_1, \dot{\gamma}_2, \dot{\gamma}_3, \dot{\gamma}_4). \tag{A.21}$$

Most of the phenomenological anisotropic plasticity theories have used either the plastic work per unit volume W^{p} or the effective plastic strain γ as the measure of the equivalent isotropic hardening state under general stress loading (Hill, 1950; Chakrabarty, 1970; Bassani, 1994; Khan and Huang, 1995; Barlat et al., 1997a,b, 2004). Motivated by Eq. (A.19) which defines the effective shear strain rate, one of the possible isotropic hardening evolution laws is

$$\dot{\xi}^{\frac{a}{a-1}} = c_1\eta_1^{\frac{1}{a-1}}\dot{\gamma}_1^{\frac{a}{a-1}} + c_2\eta_2^{\frac{1}{a-1}}\dot{\gamma}_2^{\frac{a}{a-1}} + \frac{d_3}{2}\kappa_3^{\frac{1}{a-1}}\dot{\gamma}_3^{\frac{a}{a-1}} + \frac{d_4}{2}\kappa_4^{\frac{1}{a-1}}\dot{\gamma}_4^{\frac{a}{a-1}}, \tag{A.22}$$

where the weighting coefficients c_1, c_2, d_3 and d_4 are functions of the loading orientation angle θ and they account for the effect of the planar anisotropy of the sheet metal on its isotropic hardening behavior. When all four weighting coefficients are set to 1, the isotropic hardening rate is identical to the effective shear strain rate, namely, $\dot{\xi} = \dot{\gamma}$. On the other hand, by setting $c_1 = c_2 = d_3 = d_4 = 2\bar{\eta}^{1/(a-1)}$, one has (according to Eqs. (A.16), (A.17), (A.19) and (A.22))

$$\begin{aligned}\dot{W}^{\mathrm{p}} &= 2\tau\dot{\gamma} = 2\{\bar{\eta}\dot{\gamma}\}^{\frac{1}{a-1}}\dot{\gamma} = 2\bar{\eta}^{\frac{1}{a-1}}\dot{\gamma}^{\frac{a}{a-1}} \\ &= 2\bar{\eta}^{\frac{1}{a-1}}\eta_1^{\frac{1}{a-1}}\dot{\gamma}_1^{\frac{a}{a-1}} + 2\bar{\eta}^{\frac{1}{a-1}}\eta_2^{\frac{1}{a-1}}\dot{\gamma}_2^{\frac{a}{a-1}} + \bar{\eta}^{\frac{1}{a-1}}\kappa_3^{\frac{1}{a-1}}\dot{\gamma}_3^{\frac{a}{a-1}} + \bar{\eta}^{\frac{1}{a-1}}\kappa_4^{\frac{1}{a-1}}\dot{\gamma}_4^{\frac{a}{a-1}} = \dot{\xi}^{\frac{a}{a-1}}.\end{aligned} \tag{A.23}$$

In general, no such simple identities may exist between $\dot{\xi}$ and $\dot{\gamma}$ and between $\dot{\xi}$ and $\dot{W}^{\mathrm{p}}$ for anisotropic sheet metals.

A.5. Plane stress constitutive equations in terms of anisotropic material functions

The plane-stress anisotropic plasticity model has been successfully formulated in the above section following a clear and consistent underlying physical process in terms of planar macroscopic double slips. The complete formulation of the model is summarized here (using Eqs. (A.20), (A.16), (A.22), (A.23), (A.13) and (A.15))

$$\tau = \left(\frac{1}{\eta_1}\left|\frac{\sigma_1}{2}\right|^a + \frac{1}{\eta_2}\left|\frac{\sigma_2}{2}\right|^a + \frac{1}{\bar{\kappa}}\left|\frac{\sigma_1-\sigma_2}{2}\right|^a\right)^{\frac{1}{a}}$$
(an effective stress or flow function), (A.24)

$$\dot{\gamma} = \frac{\sigma_1\dot{\varepsilon}_1 + \sigma_2\dot{\varepsilon}_2}{2\tau}$$
(the effective plastic strain rate by work equivalency), (A.25)

$$\dot{\xi} = \dot{\gamma}\left(\frac{c_1}{\eta_1}\left|\frac{\sigma_1}{2\tau}\right|^a + \frac{c_2}{\eta_2}\left|\frac{\sigma_2}{2\tau}\right|^a + \Sigma\left|\frac{\sigma_1-\sigma_2}{2\tau}\right|^a\right)^{\frac{a-1}{a}}$$
(an evolution law of isotropic hardening), (A.26)

$$\dot{W}^{\mathrm{p}} = 2\tau\dot{\gamma} = \sigma_1\dot{\varepsilon}_1 + \sigma_2\dot{\varepsilon}_2$$
(the dissipation rate of plastic work per unit volume), (A.27)

$$\dot{\varepsilon}_1 = \frac{\dot{\gamma}}{\eta_1}\left|\frac{\sigma_1}{2\tau}\right|^{a-2}\frac{\sigma_1}{2\tau} + \frac{\dot{\gamma}}{\bar{\kappa}}\left|\frac{\sigma_1-\sigma_2}{2\tau}\right|^{a-2}\frac{\sigma_1-\sigma_2}{2\tau},$$
$$\dot{\varepsilon}_2 = \frac{\dot{\gamma}}{\eta_2}\left|\frac{\sigma_1}{2\tau}\right|^{a-2}\frac{\sigma_1}{2\tau} - \frac{\dot{\gamma}}{\bar{\kappa}}\left|\frac{\sigma_1-\sigma_2}{2\tau}\right|^{a-2}\frac{\sigma_1-\sigma_2}{2\tau}, \quad \dot{\varepsilon}_3 = -\dot{\varepsilon}_1 - \dot{\varepsilon}_2,$$
(the flow rule for $\mathbf{D}^{\mathrm{p}}$), (A.28)

$$\dot{\varepsilon}_{12} = \frac{\dot{\gamma}\Delta_1}{\eta_1}\left|\frac{\sigma_1}{2\tau}\right|^{a-2}\frac{\sigma_1}{2\tau} + \frac{\dot{\gamma}\Delta_2}{\eta_2}\left|\frac{\sigma_2}{2\tau}\right|^{a-2}\frac{\sigma_2}{2\tau} + \dot{\gamma}\Delta\left|\frac{\sigma_1-\sigma_2}{2\tau}\right|^{a-2}\frac{\sigma_1-\sigma_2}{2\tau},$$
$$\dot{\omega}_{12} = -\frac{\dot{\gamma}\Delta_1}{\eta_1}\left|\frac{\sigma_1}{2\tau}\right|^{a-2}\frac{\sigma_1}{2\tau} + \frac{\dot{\gamma}\Delta_2}{\eta_2}\left|\frac{\sigma_2}{2\tau}\right|^{a-2}\frac{\sigma_2}{2\tau} + \dot{\gamma}\Psi\left|\frac{\sigma_1-\sigma_2}{2\tau}\right|^{a-2}\frac{\sigma_1-\sigma_2}{2\tau}$$
(the flow rule for $\mathbf{W}^{\mathrm{p}}$), (A.29)

$$\tau = \tau_0(\xi, \dot{\gamma}) \quad \text{(the flow condition or flow surface)}, \tag{A.30}$$

where $\tau_0(\xi, \dot{\gamma})$ is the rate-dependent effective flow strength of the sheet metal, and η_1, η_2, $\bar{\kappa}$, c_1, c_2, Σ, Δ_1, Δ_2, Δ and Ψ are 10 macroscopic material functions required by the anisotropic plasticity theory which may all depend on the loading orientation angle θ as well as the principal stresses. These material functions are related to the effective macroscopic slip variables via

$$\eta_1 \equiv \frac{\eta_1^*/\bar{\eta}}{(\sin 2\alpha_1)^a(\cos\delta_1)^{a-1}}, \quad \eta_2 \equiv \frac{\eta_2^*/\bar{\eta}}{(\sin 2\alpha_2)^a(\cos\delta_2)^{a-1}},$$
$$\kappa_3 \equiv \frac{\kappa_3^*/\bar{\eta}}{(\sin 2\beta_3)^a}, \quad \kappa_4 \equiv \frac{\kappa_4^*/\bar{\eta}}{(\sin 2\beta_4)^a}, \tag{A.31}$$
$$\frac{1}{\bar{\kappa}} \equiv \frac{1}{2\kappa_3} + \frac{1}{2\kappa_4}, \quad \Sigma \equiv \left(\frac{d_3}{2\kappa_3} + \frac{d_4}{2\kappa_4}\right),$$

$$\Delta_1 \equiv -\frac{\sin\delta_1}{2\cos\alpha_1}, \quad \Delta_2 \equiv -\frac{\sin\delta_2}{2\cos\alpha_2}, \tag{A.32}$$

$$\Delta \equiv \left(\frac{\cos 2\beta_3}{2\kappa_3\sin 2\beta_3} - \frac{\cos 2\beta_4}{2\kappa_4\sin 2\beta_4}\right), \quad \Psi \equiv \left(\frac{1}{2\kappa_3\sin 2\beta_3} - \frac{1}{2\kappa_4\sin 2\beta_4}\right). \tag{A.33}$$

In principle, once the stress exponent ($a - 1 > 0$), the effective viscosity coefficient $\bar{\eta}$, the normalized out-of-plane and in-plane shearing viscosities η and κ, the isotropic hardening weight coefficients c and d, and the slip plane angles α_1, α_2, β_3 and β_4 and the slip offset angles δ_1 and δ_2 are specified, the macroscopic slip model can be applied straightforward to describe the anisotropic plastic flow behavior of a sheet metal. In practice, the effective macroscopic slips are a useful concept to derive the resulting constitutive equations of the model, but an actual determination of the slip modes in terms of the slip plane angles α_1, α_2, β_3, β_4, δ_1 and δ_2 is in general rather difficult for an orthotropic polycrystalline sheet metal. Simple mechanical tests are thus required to directly evaluate these 11 material functions (including $\tau_0(\xi, \dot{\gamma})$). A detailed discussion on the experimental procedure of their evaluation has been given elsewhere (Tong, 2005).

Some comments on the derived flow function and the flow rules for $\mathbf{D}^{\mathrm{p}}$ and $\mathbf{W}^{\mathrm{p}}$ are in order. For a fixed loading orientation angle θ, one can show that the flow function defined by Eq. (A.24) is strictly convex in (σ_1, σ_2) space for $a > 1$, $\eta_1 > 0$, $\eta_2 > 0$, and $\bar{\kappa} > 0$ (assuming that η_1, η_2, and $\bar{\kappa}$ may be dependent on the loading orientation angle due to planar plastic anisotropy but are *independent* of the principal stresses). The four inequality conditions have clear physical underpinnings as they are related to the power-law viscous shearing flow model of the effective macroscopic slips (Eq. (A.14)). Requirements to ensure the convexity of the flow function under more general biaxial stress loading are left for further investigation. If one specifies the following conditions on the three anisotropic material functions defining the flow rule for the shear strain rate $\dot{\varepsilon}_{12}$ in Eq. (A.28c)

$$\Delta_1 = -\frac{\eta_1'(\theta)}{\eta_1(\theta)} \frac{\sigma_1}{4a(\sigma_1 - \sigma_2)}, \quad \Delta_2 = -\frac{\eta_2'(\theta)}{\eta_2(\theta)} \frac{\sigma_2}{4a(\sigma_1 - \sigma_2)},$$
$$\Delta = -\frac{1}{4a} \frac{\bar{\kappa}'(\theta)}{\bar{\kappa}^2(\theta)}, \tag{A.34}$$

then Eq. (A.28) is the *associated* flow rule of plastic strain rates using the flow potential given by Eq. (24). The formulas for the associated flow rule in terms of the so-called intrinsic variables σ_1, σ_2, and θ have been given by Hill (1980, 1990) as

$$\dot{\varepsilon}_1 = \lambda \frac{\partial \tau}{\partial \sigma_1}, \quad \dot{\varepsilon}_2 = \lambda \frac{\partial \tau}{\partial \sigma_2}, \quad \dot{\varepsilon}_{12} = \frac{\lambda}{2(\sigma_1 - \sigma_2)} \frac{\partial \tau}{\partial \theta}, \tag{A.35}$$

where $\lambda = \dot{\gamma}$ from the work equivalency requirement.

The *continuity condition* on the flow function at equal biaxial loading as one approaches it from various loading orientation angles requires

$$\frac{1}{\eta_1(\theta)} + \frac{1}{\eta_2(\theta)} = \left(\frac{2\tau}{\sigma_B}\right)^a, \quad \text{so,} \frac{\eta_1'(\theta)}{\eta_1^2(\theta)} + \frac{\eta_1'(\theta)}{\eta_2^2(\theta)} = 0, \tag{A.36}$$

where both the effective flow strength $\tau = \tau_0(\xi, \dot{\gamma})$ and the flow stress under equal biaxial tension $\sigma_B(\xi, \dot{\gamma})$ are independent of the loading orientation angle θ. A similar continuity condition exists also for the evolution law of isotropic hardening equation (A.26) under equal biaxial loading

$$\frac{c_1(\theta)}{\eta_1(\theta)}+\frac{c_2(\theta)}{\eta_2(\theta)}=\frac{c_1(0)}{\eta_1(0)}+\frac{c_2(0)}{\eta_2(0)}. \tag{A.37}$$

If furthermore the *smoothness* of the flow function is desired (such as corners or vertices are not allowed), one may impose a continuity condition on the flow surface normal at equal biaxial loading. That is, the flow rules Eqs. (A28) and (29) are *assumed* to be valid for any loading orientation angles under equal biaxial loading $\sigma_1=\sigma_2=\sigma_B$ (although the loading orientation angle is zero according to the convention defined in Section A.4)

$$\begin{aligned}
\dot{\varepsilon}_1&=\frac{\dot{\gamma}}{\eta_1(\theta)}\left|\frac{\sigma_B}{2\tau}\right|^{a-2}\frac{\sigma_B}{2\tau}=\frac{\dot{\varepsilon}_1^0+\dot{\varepsilon}_2^0}{2}+\frac{\dot{\varepsilon}_1^0-\dot{\varepsilon}_2^0}{2}\cos 2\theta,\\
\dot{\varepsilon}_2&=\frac{\dot{\gamma}}{\eta_2(\theta)}\left|\frac{\sigma_B}{2\tau}\right|^{a-2}\frac{\sigma_B}{2\tau}=\frac{\dot{\varepsilon}_1^0+\dot{\varepsilon}_2^0}{2}-\frac{\dot{\varepsilon}_1^0-\dot{\varepsilon}_2^0}{2}\cos 2\theta,\\
\dot{\varepsilon}_{12}&=\dot{\gamma}\left(\frac{\Delta_1(\theta)}{\eta_1(\theta)}+\frac{\Delta_2(\theta)}{\eta_2(\theta)}\right)\left|\frac{\sigma_B}{2\tau}\right|^{a-2}\frac{\sigma_B}{2\tau}=-\frac{\dot{\varepsilon}_1^0-\dot{\varepsilon}_2^0}{2}\sin 2\theta,\\
\dot{\omega}_{12}&=\dot{\gamma}\left(-\frac{\Delta_1(\theta)}{\eta_1(\theta)}+\frac{\Delta_2(\theta)}{\eta_2(\theta)}\right)\left|\frac{\sigma_B}{2\tau}\right|^{a-2}\frac{\sigma_B}{2\tau}=0\quad\text{(zero plastic spin)},
\end{aligned} \tag{A.38}$$

where $\dot{\varepsilon}_1^0$ and $\dot{\varepsilon}_2^0$ are the principal plastic strain rates under equal biaxial loading and the 2D coordinate transformation of strain rates from the principal axes of stress and strain rates to the loading orientation angle θ is also included in Eq. (A.38). One obtains from Eq. (A.38)

$$\begin{aligned}
\frac{\eta_1(\theta)}{\eta_2(\theta)}&=\frac{\dot{\varepsilon}_1^0+\dot{\varepsilon}_2^0-\left(\dot{\varepsilon}_1^0-\dot{\varepsilon}_2^0\right)\cos 2\theta}{\dot{\varepsilon}_1^0+\dot{\varepsilon}_2^0+\left(\dot{\varepsilon}_1^0-\dot{\varepsilon}_2^0\right)\cos 2\theta}=\frac{1+\Omega_0-(1-\Omega_0)\cos 2\theta}{1+\Omega_0+(1-\Omega_0)\cos 2\theta},\\
\frac{\Delta_1(\theta)}{\eta_1(\theta)}&=\frac{\Delta_2(\theta)}{\eta_2(\theta)}=-\frac{\left(\dot{\varepsilon}_1^0-\dot{\varepsilon}_2^0\right)\sin 2\theta}{4\dot{\varepsilon}_1^0\eta_1(0)}=-\frac{(1-\Omega_0)\sin 2\theta}{4\eta_1(0)},
\end{aligned} \tag{A.39}$$

where $\Omega_0=\dot{\varepsilon}_2^0/\dot{\varepsilon}_1^0$ is the plastic strain ratio under equal biaxial loading. Finally, by combining Eqs. (A.36) and (A.39), one has

$$\begin{aligned}
\frac{1}{\eta_1(\theta)}&=\frac{1}{\eta_2(\theta+\pi/2)}=\left(\frac{1}{2}+\frac{1-\Omega_0}{1+\Omega_0}\frac{\cos 2\theta}{2}\right)\left(\frac{2\tau}{\sigma_B}\right)^a,\\
\frac{\Delta_1(\theta)}{\eta_1(\theta)}&=\frac{\Delta_2(\theta)}{\eta_2(\theta)}=-\frac{1-\Omega_0}{1+\Omega_0}\frac{\sin 2\theta}{4}\left(\frac{2\tau}{\sigma_B}\right)^a.
\end{aligned} \tag{A.40}$$

References

Banabic, D., Aretz, H., Comsa, D.S., Paraianu, L., 2005. An improved analytical description of orthotropy in metallic sheets. I. J. Plasticity 21 (3), 493–512.

Barlat, F., 1987. Crystallographic texture, anisotropic yield surfaces and forming limits of sheet metals. Mater. Sci. Eng. 91, 55–72.

Barlat, F., Richmond, O., 1987. Prediction of tricomponent plane stress yield surfaces, associated flow and failure behavior of strongly textured F.C.C. polycrystalline sheets. Mater. Sci. Eng. 95, 15–29.

Barlat, F., Lian, J., 1989. Plastic behavior and stretchability of sheet metals, Part I: a yield function for orthotropic sheets under plane stress conditions. Int. J. Plasticity 5, 51–56.

Barlat, F., Lege, D.J., Brem, J.C., 1991. A six-component yield function for anisotropic materials. Int. J. Plasticity 7, 693–712.

Barlat, F., Becker, R.C., Hayashida, Y., Maeda, Y., Yanagawa, M., Chung, K., Brem, J.C., Lege, D.J., Matsui, K., Murtha, S.J., Hattori, S., 1997a. Yield description for solution strengthened aluminum alloys. Int. J. Plasticity 13 (4), 385–401.

Barlat, F., Maeda, Y., Chung, K., Yanagawa, M., Brem, J.C., Hayashida, Y., Lege, D.J., Matsui, K., Murtha, S.J., Hattori, S., Becker, R.C., Makosey, S., 1997b. Yield function development for aluminum alloy sheets. J. Mech. Phys. Solids 45 (11/12), 1727–1763.

Barlat, F., Brem, J.C., Yoon, J.W., Chung, K., Dick, R.E., Lege, D.J., Pourboghrat, F., Choi, S.H., Chu, E., 2004. Plane stress yield function for aluminum alloy sheets: Part 1. Theory I. J. Plasticity 20 (3), 495–522.

Barlat, F., Aretz, H., Yoon, J.W., Karabin, M.E., Brem, J.C., Dick, R.E., 2005. Linear transfomation-based anisotropic yield functions. I. J. Plasticity 21 (5), 1009–1039.

Bassani, J.L., 1977. Yield characterization of metals with transversely isotropic plastic properties. Int. J. Mech. Sci. 19, 651–660.

Bassani, J.L., 1994. Plastic flow of crystals. Adv. Appl. Mech. 30, 191–258.

Bishop, J.W.F., Hill, R., 1951a. A theory of the plastic distortion of a polycrystalline aggregates under combined stresses. Philos. Mag. 42, 414–427.

Bishop, J.W.F., Hill, R., 1951b. A theoretical derivation of the plastic properties of polycrystalline face-centered metals. Philos. Mag. 42, 1298–1307.

Bourne, L., Hill, R., 1950. On the correlation of the directional properties of rolled sheet in tension and cupping tests. Philos. Mag. 41, 671–681.

Bron, F., Besson, J., 2004. A yield function for anisotropic materials: application to aluminum alloys. I. J. Plasticity 20 (4/5), 937–963.

Budiansky, B., 1984. Anisotropic plasticity of plane-isotropic sheets. In: Dvorak, G.J., Shield, R.T. (Eds.), Mechanics of Material Behavior, Studies in Applied Mechanics, vol. 6. Elsevier, Amsterdam, pp. 15–29.

Bunge, H.J., Nielsen, I., 1997. Experimental determination of plastic spin in polycrystalline materials. Int. J. Plasticity 13 (5), 435–446.

Cao, J., Yao, H., Karafillis, A., Boyce, M.C., 2000. Prediction of localized thinning in sheet metal using a general anisotropic yield criterion. Int. J. Plasticity 16, 1105–1129.

Chakrabarty, J., 1970. A hypothesis of strain-hardening in anisotropic plasticity. Int. J. Mech. Sci. 12, 169–176.

Cazacu, O., Barlat, F., 2001. Generalization of Drucker's yield criterion to orthotropy. Math. Mech. Solids 6, 613–630.

Chung, K., Lee, M., Kim, D., Kim, C., Wenner, M.L., Barlat, F., 2005. Spring-back evaluation of automotive sheets based on isotropic-kinematic hardening laws and non-quadratic anisotropic yield functions: Part I: theory and formulation. I. J. Plasticity 21 (5), 861–882.

Dafalias, Y.F., 1985. The plastic spin. J. Appl. Mech. 52, 865.

Dafalias, Y.F., 2000. Orientational evolution of plastic orthotropy in sheet metal. J. Mech. Phys. Solids 48, 2231–2255.

Dodd, B., Caddell, R.M., 1984. On the anomalous behavior of anisotropic sheet metals. Int. J. Mech. Sci. 26, 113–118.

Eisenberg, M.A., Yen, C.F., 1981. A theory of multiaxial anisotropic viscoplasticity. Trans. ASME J. Appl. Mech. 48, 276–284.

Gotoh, M., 1977. A theory of plastic anisotropy based on a yield function of fourth order (plane stress state). Int. J. Mech. Sci. 19, 505–512.

Graf, A., Hosford, W.F., 1993. Effect of changing strain paths on forming limit diagrams of Al-2008-T4. Metall. Trans. A 24, 2503.

Graf, A., Hosford, W.F., 1994. The influence of strain path changes on forming limit diagrams of Al-6111-T4. Int. J. Mech. Sci. 36, 897–910.
Hill, R., 1948. A theory of the yielding and plastic flow of anisotropic metals. Proc. R. Soc. Lond. A 193, 281–297.
Hill, R., 1950. The Mathematical Theory of Plasticity. Clarendon Press, Oxford.
Hill, R., 1979. Theoretical plasticity of textured aggregates. Math. Proc. Cambridge Philos. Soc. 85, 179–191.
Hill, R., 1980. Basic stress analysis of hyperbolic regimes in plastic media. Math. Proc. Cambridge Philos. Soc. 88, 359–369.
Hill, R., 1990. Constitutive modeling of orthotropic plasticity in sheet metals. J. Mech. Phys. Solids 38, 405–417.
Hill, R., 1991. A theoretical perspective on in-plane forming of sheet metals. J. Mech. Phys. Solids 39, 295–307.
Hill, R., 1993. A user-friendly theory of orthotropic plasticity in sheet metals. Int. J. Mech. Sci. 35, 19–25.
Hosford, W.F., 1985. Comments on anisotropic yield criteria. Int. J. Mech. Sci. 27, 423–427.
Hosford, W.F., 1993. The Mechanics of Crystals and Textured Polycrystals. Oxford University Press, Oxford.
Hosford, W.F., Caddell, R.M., 1993. Metal Forming: Mechanics and Metallurgy, second ed. Prentice-Hall, Englewood Cliffs, NJ.
Jones, S.E., Gillis, P.P., 1984. A generalized quadratic flow law for sheet metals. Metall. Trans. A 15, 129–132.
Hu, W., 2005. An orthotropic yield criterion in a 3-D general stress state. I. J. Plasticity 21 (9), 1771–1796.
Karafillis, A.P., Boyce, M.C., 1993. A general anisotropic yield criterion using bounds and a transformation weighting tensor. J. Mech. Phys. Solids 41, 1859–1886.
Khan, A.S., Huang, S., 1995. Continuum Theory of Plasticity. Wiley, New York.
Kim, K.H., Yin, J.J., 1997. Evolution of anisotropy under plane stress. J. Mech. Phys. Solids 45 (5), 841–851.
Kuwabara, T., Kuroda, M., Tvergaard, V., Nomura, K., 2000. Use of abrupt strain path change for determining subsequent yield surface: experimental study with metal sheets. Acta Mater. 48, 2071–2079.
Lademo, O.-G., Hopperstad, O.S., Langseth, M., 1999. An evaluation of yield criteria and flow rules for aluminum alloys. Int. J. Plasticity 15, 191–208.
Lin, S.B., Ding, J.L., 1996. A modified form of Hill's orientation-dependent yield criterion for orthotropic sheet metals. J. Mech. Phys. Solids 44, 1739–1764.
Logan, R.W., Hosford, W.F., 1980. Upper-bound anisotropic yield locus calculations assuming ⟨1 1 1⟩ pencil glide. Int. J. Mech. Sci. 22, 419–430.
Lubliner, J., 1990. Plasticity Theory. Macmillan, New York.
McDowell, D.L., Moosbrugger, J.C., 1992. Continuum slip foundation of elasto-viscoplasticity. Acta Mech. 93, 73–87.
Mellor, P.B., 1982. Experimental studies of plastic anisotropy in sheet metal. In: Hopkins, H.G., Sewell, M.J. (Eds.), Mechanics of Solids – The Rodney Hill 60th Anniversary Volume. Pergamon Press, Oxford, pp. 383–415.
Montheillet, F., Jonas, J.J., Benferrah, M., 1991. Development of anisotropy during the cold rolling of aluminum sheet. Int. J. Mech. Sci. 33, 197–209.
Pearce, R., 1968. Some aspects of anisotropic plasticity in sheet metals. Int. J. Mech. Sci. 10, 995–1005.
Phillips, A., Liu, C.S., Justusson, J.W., 1972. An experimental investigation of yield surfaces at elevated temperature. Acta Mech. 14, 119–146.
Rata-Eskola, A.J., 1979. On the stress state dependence of the strain-hardening of anisotropic sheet steel. Metall. Trans. A 10, 1949.
Rice, J.R., 1971. Inelastic constitutive relations for solids: an internal-variable theory and its application to metal plasticity. J. Mech. Phys. Solids 19, 433–455.
Stoughton, T.B., 2002. A non-associated flow rule for sheet metal forming. Int. J. Plasticity 18, 687–714.
Tong, W., 2003. A planar plastic flow theory for monoclinic sheet metals. Int. J. Mech. Sci. (submitted).

Tong, W., Zhang, N., Xie, C., 2003. Modeling of anisotropic plastic flows of automotive sheet metals. In: Das, S.K. (Ed.), Aluminum 2003. The Minerals, Metals, & Materials Society, pp. 193–202.

Tong, W., Tao, H., Jiang, X., 2004. Modeling of rotation of orthotropic symmetry axes of sheet metals subjected to off-axis tension. ASME Trans. J. Appl. Mech. 71 (4), 521–531.

Tong, W., 2005. A planar plastic flow theory of orthotropic sheets and the experimental procedure for its evaluations. Proc. R. Soc. Lond. A 461, 1775–1809.

Van Houtte, P., Van Bael, A., 2004. Convex plastic potentials of fourth and sixth rank for anisotropic materials. I. J. Plasticity 20 (8–9), 1505–1524.

Vial, C., Hosford, W.F., Caddel, R.M., 1983. Yield loci of anisotropic sheet metals. Int. J. Mech. Sci. 25 (12), 899–915.

Wagoner, R.H., Wang, N.-M., 1979. An experimental and analytical investigation of in-plane deformation of 2036-T4 aluminum sheet. Int. J. Mech. Sci. 21, 255–264.

Woodthorpe, J., Pearce, R., 1970. The anomalous behavior of aluminum sheet under balanced biaxial tension. Int. J. Mech. Sci. 12, 341–347.

Wu, H.C., Hong, H.K., Shiao, Y.P., 1999. Anisotropic plasticity with application to sheet metals. Int. J. Mech. Sci. 41, 703–724.

Wu, H.C., 2002. Anisotropic plasticity for sheet metals using the concept of combined isotropic-kinematic hardening. Int. J. Plasticity 18, 1661–1682.

Wu, P.D., Jain, M., Savoie, J., MacEwen, S.R., Tugcu, P., Neale, K.W., 2003. Evaluation of anisotropic yield functions for aluminum sheets. Int. J. Plasticity 19, 121–138.

Yao, H., Cao, J., 2002. Prediction of forming limit curves using an anisotropic yield function with prestrain induced backstress. Int. J. Plasticity 18, 1013–1038.

Yoon, J.W., Barlat, F., Dick, R.E., 1999. Sheet metal forming simulation for aluminum alloy sheetsSheet Metal Forming Simulation: Sing-Tang 65th Anniversary Volume, SAE paper 2000-01-0774. Society of Automotive Engineers, p. 67.

Young, R.F., Bird, J.E., Duncan, J.L., 1981. An automated hydraulic bulge tester. J. Appl. Metalworking 2, 11–18.